haematologica
Journal of The Ferrata Storti Foundation

Long non-coding RNA mitophagy and ALK- anaplastic lymphoma associated transcript: a novel regulator of mitophagy in T cell lymphoma

by Valentina Mularoni, Benedetta Donati, Annalisa Tameni, Veronica Manicardi, Francesca Reggiani, Elisabetta Sauta, Magda Zanelli, Marco Tigano, Emanuele Vitale, Federica Torricelli, Stefano Ascani, Giovanni Martino, Giorgio Inghirami, Francesca Sanguedolce, Alessia Ruffini, Alberto Bavieri, Stefano Luminari, Marco Pizzi, Angelo Paolo Dei Tos, Cinzia Fesce, Antonino Neri, Alessia Ciarrocchi, and Valentina Fragliasso

Received: December 14, 2022.
Accepted: June 20, 2023.

Citation: Valentina Mularoni, Benedetta Donati, Annalisa Tameni, Veronica Manicardi, Francesca Reggiani, Elisabetta Sauta, Magda Zanelli, Marco Tigano, Emanuele Vitale, Federica Torricelli, Stefano Ascani, Giovanni Martino, Giorgio Inghirami, Francesca Sanguedolce, Alessia Ruffini, Alberto Bavieri, Stefano Luminari, Marco Pizzi, Angelo Paolo Dei Tos, Cinzia Fesce, Antonino Neri, Alessia Ciarrocchi, and Valentina Fragliasso. Long non-coding RNA mitophagy and ALK- anaplastic lymphoma associated transcript: a novel regulator of mitophagy in T cell lymphoma. Haematologica. 2023 June 29. doi: 10.3324/haematol.2022.282552 [Epub ahead of print]

Long non-coding RNA mitophagy and ALK$^-$ anaplastic lymphoma associated transcript: a novel regulator of mitophagy in T cell lymphoma

Valentina Mularoni[1], Benedetta Donati[1], Annalisa Tameni[1], Veronica Manicardi[1], Francesca Reggiani[1], Elisabetta Sauta[2], Magda Zanelli[3], Marco Tigano[4], Emanuele Vitale[1, 5], Federica Torricelli[1], Stefano Ascani[6], Giovanni Martino[6,7], Giorgio Inghirami[8], Francesca Sanguedolce[9], Alessia Ruffini[10], Alberto Bavieri[10], Stefano Luminari[10], Marco Pizzi[11], Angelo Paolo Dei Tos[11], Cinzia Fesce[12], Antonino Neri[13], Alessia Ciarrocchi[1], Valentina Fragliasso[1,#]

Affiliations

1 Laboratory of Translational Research, Azienda USL-IRCCS di Reggio Emilia, Viale Risorgimento 80, 42123, Reggio Emilia, Italy

2 IRCCS Humanitas Clinical and Research Center, via Manzoni 56, 20089, Rozzano, Milan, Italy.

3 Pathology Unit, Department of Oncology, Azienda Unità Sanitaria Locale - IRCCS di Reggio Emilia, Reggio Emilia, 42123, Italy.

4 Sidney Kimmel Medical College, Thomas Jefferson University, Philadelphia, PA, 19144, USA

5 Clinical and Experimental Medicine Ph.D. Program, University of Modena and Reggio Emilia, Modena, 41125, Italy.

6 Pathology Unit, Azienda Ospedaliera Santa Maria di Terni, University of Perugia, 05100 Terni, Italy.

7 Institute of Hematology and CREO, University of Perugia, Perugia 06129, Italy

8 Department of Pathology and Laboratory Medicine, Weill Cornell Medicine, New York, NY, 10065, USA.

9 Pathology Unit, Policlinico Riuniti, University of Foggia, 71122 Foggia, Italy.

10 Hematology Unit, Azienda USL-IRCCS di Reggio Emilia, 42123 Reggio Emilia, Italy.

11 Surgical Pathology & Cytopathology Unit, Department of Medicine-DIMED, University of Padova, 35128 Padova, Italy.

12 Hematology Unit, University Hospital, 71122 Foggia, Italy

13 Scientific Directorate, Azienda USL-IRCCS di Reggio Emilia, Viale Umberto I 50, 42123, Reggio Emilia, Italy

Author's contributions

V.M. and A.T. performed experiments and analyzed data, B.D. performed gene expression and Nanostring analysis, V.M., F.T., E.S., E.V. performed RNA-seq, ChIP-seq, and bioinformatics analyses. F.R. performed FACS analyses and cell sorting experiments, M.Z., S.A., G.I., F.S. C.F., M.P., A.R., G.M, S.L., A.P.D.S., and A.B. provided tissue samples and lymphoma diagnosis. M.T. and A.N. provided important experimental and analytic support. A.C. interpreted the results and helped to discuss the results. V.F. designed the project, interpreted the results, and wrote the manuscript. All the authors read and approved the final version of the manuscripts.

Disclosures

No conflicts of interest to disclose.

Running head

Transcriptional role of lncRNA MTAAT in Lymphoma

#**Corresponding author**

Valentina Fragliasso, Laboratory of Translational Research, Azienda USL-IRCCS di Reggio Emilia, Viale Risorgimento 80, 42123, Reggio Emilia, Italy. Phone: +39-0522295914; Email: Valentina.Fragliasso@ausl.re.it

Data sharing statement

All data generated and/or analyzed in this study are included in this article and its Online Supplementary Appendix. The MTAAT sequence has been deposited in the GenBank database with the accession number OM642832. Gene expression profile data are available at the Gene Expression Omnibus (GEO) repository (accession number: GSE217426).

RNA-seq raw data in fastq.gz format are available in the ArrayExpress repository, dataset E-MTAB-12462 (https://www.ebi.ac.uk/arrayexpress/experiments/E-MTAB-12462).

Word count

Abstract: 145 words

Main text: 3.650 words

6 main figures

1 supplementary file associated with the manuscript.

Acknowledgments

The authors are grateful to Marina Grassi, Ione Tamagnini, Gloria Venturini, and Riccardo Fuoco for technical help and to all the members of the laboratory for helpful discussion. V.M. and A.T. were supported by Fondazione AIRC per la Ricerca sul Cancro (AIRC). F.R. was supported by Fondazione Umberto Veronesi, V.M. and A.R. were supported by Fondazione GRADE Onlus. This study was funded by the Italian Ministry of Health through Ricerca Finalizzata (No. GR-2016-02364298, V.F.), Bando per la Valorizzazione della Ricerca

Istituzionale 2021- fondi 5 per Mille 2020 (V.F.) and Fondazione AIACE (V.F.). This study was partially supported by the Italian Ministry of Health-Ricerca Corrente Annual Program 2024.

Abstract

Long noncoding RNAs (lncRNAs) are emerging as powerful and versatile regulators of transcriptional programs and distinctive biomarkers of T-cell Lymphoma progression disease. Their role in the aggressive ALK$^-$ Anaplastic Large Cell Lymphoma (ALCL) subtype has been only in part elucidated. Starting from our previously identified ALCL-associated lncRNA signature and performing digital gene expression profiling of a retrospective cohort of ALCLs, we defined an 11 lncRNA signature able to discriminate among ALCL subtypes. We selected a not previously characterized lncRNA, MTAAT, with an ALK$^-$ ALCL preferential expression, for molecular and functional studies. We demonstrated that lncRNA MTAAT contributes to an aberrant mitochondrial turnover restraining mitophagy and promoting cellular proliferation. Functionally, lncRNA MTAAT acts as a repressor of a set of genes related to mitochondria quality control via chromatin reorganization.

Collectively, our work demonstrates the transcriptional role of lncRNA MTAAT in orchestrating a complex transcriptional program sustaining ALK$^-$ ALCL progression.

Introduction

T-cell lymphoma (TCL) is a complex and heterogeneous group of neoplasms with different biology and outcome[1]. Its diagnostic classification is still a challenge making its treatment sub-optimal. ALK$^-$ Anaplastic Large cell Lymphoma (ALCL) is one of the most aggressive T-cell lymphoma subtypes characterized by dismal prognosis and high mortality[2–4]. The molecular details of ALK$^-$ ALCL pathogenesis are largely unknown, thus limiting the

development of targeted strategies[5]. Therefore, clarifying the mechanisms underlying this disease is of utmost importance. The fast and massive implementation of deep sequencing technologies has highlighted the role of the non-coding genome in regulating cancer proliferation, especially in complex tumors without a clear genetic driver[6,7]. Particular attention has been paid to a family of transcripts of about 200bp with no coding potential known as long non-coding RNAs (lncRNAs)[8]. LncRNAs possess the striking ability to interact with protein-coding and non-coding transcripts regulating and integrating a complex network of processes simultaneously[9–12]. Thanks to their peculiar and versatile features, lncRNAs are able to influence – in a context-dependent manner – several aspects of cancer biology like cellular proliferation, apoptosis, metabolic reprogramming, genomic instability, drug resistance, invasion, and metastasis[13,14]. Thus, deregulating the expression of certain lncRNAs can directly influence the pathogenesis and/or progression of different types of cancers, including T-cell lymphoma[15].

Previously, we investigated the contribution of lncRNAs to ALCL pathogenesis by performing deep transcriptomic profiling of a cohort of ALCLs. We identified a unique set of 18 lncRNAs overexpressed in neoplastic T-lymphocytes compared to normal T-lymphocytes[16]. We were able to show that among those, lncRNA *BlackMamba* acts as a major transcriptional regulator of neoplastic T-lymphocytes in the ALK$^-$ALCL subtype, influencing lymphoma progression[16,17]. Therefore, the identified lncRNAs are not only distinctive biomarkers of disease but play relevant functional roles in the biogenesis of ALCL.

In this work, we expand our knowledge regarding lncRNAs' functional relevance in the development and progression of ALCL. Starting from our previously identified lncRNA signature and integrating the gene expression profiles (GEPs) of a large cohort of ALCL patients with clinical information, we defined a powerful lncRNA signature that discriminates between ALK$^-$ and ALK$^+$ subtypes. Then, we focused on the XLOC_211989 transcript – which resulted specifically associated with the ALK$^-$ ALCL subtype – and we characterized its

function by using multiple functional approaches. Our data suggest that this noncoding transcript coordinates the expression of a set of genes involved in mitochondrial homeostasis and mitophagy promoting lymphoma cell survival. We named this novel lncRNA *MiTophagy and ALK- Anaplastic Lymphoma Associated Transcript* (MTAAT).

Methods

Patients' specimen

Fresh and viable cryopreserved cells and formalin-fixed paraffin-embedded (FFPE) sections of two retrospective cohorts of ALCL were isolated from diagnostic/relapsed primary lymphoma biopsies. Diagnoses were assigned according to the WHO classification[1]. Tissues used for expression analyses were selected for their high tumor cell content (>50%). The FFPE cohort of ALCL included 54 cases whereas the freshly frozen cohort included 18 ALCL cases. Regarding clinicopathological characteristics of the FFPE cohort eligible for the analysis (n=44): among ALK^- ALCL, 17/29 (59%) patients were male and the median age was 70 years (range 31-88). Regarding ALK^+ ALCL, 8/15 (53%) patients were male and the median age was 39 years (range 21-75). Considering follow-up data available for 29/44 patients, the median follow-up of the cohort was 44 months (range, 2.2-152 months). The 4-year progression-free survival (PFS) rate was 70.6% (95%CI 55.2 to 90.3). The freshly frozen cohort of ALCL and immunophenotypic features of resting and donor CD4+ T-lymphocytes have been previously described[16].

The study was approved through institutional human ethics review boards of the Ethical Committee AVEN and AUSL-IRCCS di Reggio Emilia (287/2018/OSS/IRCCSRE), and patients provided written informed consent in accordance with the Declaration of Helsinki.

RNA extraction and quantitative PCR (RT-qPCR)

Total RNA from cells was extracted by TRIzol (Thermo Fisher Scientific) according to the manufacturer's instructions. One microgram of total RNA was retrotranscribed using the iScript cDNA kit, (Biorad). The amplified transcript level of each specific gene was normalized on the CHMP2A housekeeping gene. ΔΔCt quantification method was used for RT-qPCR analyses. The list of primers used is provided in **supplementary table 1**.

Antisense LNA GapmeRs transfection

MAC2A and TLBR-2 cells (1×10^6) were transfected with 50nM Antisense LNA GapmeRs concentration for a single KD. Antisense LNA GapmeR transfections were performed using the Cell Line Nucleofector Kit SF and Amaxa 4D Nucleofector (program DS-130 for TLBR-2, FI115 for MAC2A). Twenty-four hours after transfection, cells were harvested and plated 2.5×10^5 cells/ml. Antisense LNA GapmeR Negative Control (Cat. No. / ID: 33951, Qiagen) was used as a negative control. For lncRNA_211989/MTAAT we used 2 different GapmeRs (Cat. No. / ID: 339511, Qiagen), and their sequences are provided in **supplementary table 2**.

Mitochondria staining

Mitochondria were stained with Mitotracker (Thermo Fisher Scientific) accordingly to manufacturer instructions. Cells were then harvested, fixed in 4% PFA in PBS 1X for 10 min at room temperature, and spotted on glass slides using Cytospin (Thermo Scientific) as previously reported[18]. Dots were washed in PBS 1X for three times and nuclei were stained with DAPI.

Tetramethylrhodamine Methyl Ester Perchlorate (TMRM) staining was performed accordingly to manufacturer instructions (Thermo Fisher Scientific) and without substantial changes. Cells were then harvested and washed one time in RPMI media without serum. Membrane

potential was immediately measured by flow cytometry with FACSCanto™ II Cell Analyzer (BD Biosciences).

Statistical analysis

Statistical analyses were performed using GraphPad Prism Software (GraphPad). Statistical significance was determined using Student's t-test. Each experiment was replicated multiple times (>3 up to 6). All analyses were performed using R software version 4.1.3.

Results

XLOC_211989 is a novel biomarker that stratifies ALK$^-$ALCL patients

We assessed whether the previously generated ALCL-associated lncRNA-signature[16] might be used to distinguish ALCL subtypes in a retrospective cohort of 54 ALCL cases. Gene expression analyses were performed by digital multiplexing profiling using a custom panel of probes targeting the 17 previously identified lncRNAs and four additional genes used for the molecular classification of ALCL subtypes[19].

Out of the 54 total samples, 44 ALCLs GEPs passed stringent quality controls and resulted eligible for the analysis (**Figure 1A)**. 15/44 (34%) samples were classified as ALK$^+$ALCL and 29/44 (66%) samples scored as ALK$^-$ALCL **(Figure 1A, Supplementary Figures 1A-B, Supplementary Table 4).** Focusing on lncRNAs, we confirmed that 17/17 (100%) lncRNAs were expressed in the ALCL cohort. Principal Component Analysis (PCA) showed that lncRNA expression profiles well segregated ALK$^+$ and ALK$^-$ ALCL samples (**Figure 1B**) resulting in 11 of the 17 (65%) lncRNAs significantly deregulated between the two subtypes (**Figure 1C, Supplementary Figure 1C**). In particular: 7 lncRNAs were over-expressed in ALK$^-$ ALCL patients while 4 lncRNAs were over-expressed in ALK$^+$ ALCL patients (**Figure 1C**). According to our previously observations[16], lncRNA *BlackMamba* showed a significant and negative correlation with ALK expression (**Figure 1C)**.

We focused our attention on the six uncharacterized lncRNAs that were significantly associated with ALK$^-$ subtype (**Figure 1D)**. First, we confirmed their association with the ALK$^-$ subtype by targeted RT-qPCR performed in a previously published cohort of 15 freshly frozen ALCL[16]. From this analysis, XLOC_211989 – herein named lncRNA MTAAT – showed the strongest and most significant association with ALK$^-$ALCL (**Figures 1D-E, Supplementary Figure 1D)**. No detectable MTAAT expression was observed in donor resting or activated CD4+ cells (**Supplementary Figure 1E**) further confirming ALCL-restricted MTAAT expression.

To strengthen these observations, we explored the correlation between MTAAT and ALK expression in the retrospective cohort of ALCLs. Linear regression analysis showed that MTAAT was inversely correlated with ALK expression and positively correlated with lncRNA BlackMamba (**Figure 1F**). ROC curve for ALK subtype classification showed that MTAAT has a high capacity (70%) to discriminate between ALK$^-$ and ALK$^+$ patients (AUC 0.70 0.54-0.85) (**Figure 1G, Supplementary Figure 1F**).

MTAAT promoter is bound by RNA Polymerase II and enriched for active histone marks

Genomic annotation showed that the MTAAT sequence matches an uncharacterized intergenic transcript encoded on the plus strand of chromosome 3 with an estimated transcript length of 7,189 bp and no predicted alternative isoforms (**Figure 2A**). *In silico* analysis predicted four potential open reading frames (ORFs) with irrelevant coding potential within MTAAT sequence, confirming the non-coding nature of this transcript (**Supplementary Table 5**).

Given the specificity of MTAAT expression in the ALK$^-$ALCL subtype, we sought to define *in vitro* the molecular mechanisms that control its expression. For this analysis, we chose the two ALK$^-$ALCL cell lines – TLBR2 and MAC2A – displaying the highest levels of MTAAT

expression (**Supplementary Figure 2A**). To identify the promoter of MTAAT, we first analyzed RNAPII genomic occupancy and histone 3 trimethyl lysine 4 (H3K4me3) profile using the Chromatin Immunoprecipitation followed by sequencing (ChIP-seq) in TLBR-2 cells. A high-density distribution of RNAPII within a 2000 bp region spanning the putative transcription start site (TSS) of MTAAT (P3-P6) was observed. This region was also enriched in H3K4me3 confirming the promoter-like nature of its sequence (**Figure 2A**). We confirmed the findings by ChIP-qPCR in both TLBR-2 and MAC2A cell lines **(Figures 2B-C, Supplementary Figure 2B)**. We also showed that this region is marked by a high level of histone H3 acetyl-lysine 27 (H3K27ac) confirming that this locus is transcriptionally active in these cellular models (**Figure 2D, Supplementary Figure 2B**). Notably, ChIP-qPCR analysis did not show RNAPII or histone modifications enrichment in a cell line - CUTLL1 - negative for MTAAT expression **(Supplementary Figure 2C)**, validating the specificity of our observations. To assess whether MTAAT putative promoter is able to transactivate transcription, we cloned the 2000bp DNA sequence spanning from −1,500bp to +500 bp of MTAAT-TSS upstream of a luciferase reporter cassette. In this "promoter-like" configuration, high luciferase activity was detected in both MAC2A and TLBR-2 cells (**Figure 2E**).

Next, we asked what are the signaling pathways underlying MTAAT expression. Based on the genomic profiles observed in ChIP-seq, we selected a 500bp region spanning the TSS of MTAAT and performed a motif search analysis to identify potential transcriptional factors (TFs) binding sites. For this, we used the FIMO analysis pipeline[20] and identified 117 hypothetical TFs **(Supplementary Table 6)**. Notably, some TFs – including STATs, GATAs, and IRFs – were pertinent to signaling pathways known to be active and deregulated in ALK$^-$ ALCL[5] (**Figure 2F**). Specifically, we found a significant enrichment of several pathways related to the cellular response to cytokines, interferon, interleukins, and regulation of T-cell differentiation.

MTAAT is a chromatin-associated lncRNA essential for the transcriptional control of mitochondrial processes

To examine the biological role of MTAAT in T-cell lymphoma, we first studied MTAAT cellular localization performing sub-cellular fractionation. We found that MTAAT was enriched in the nucleus and strongly associated with the chromatin fraction of lymphoma cells (**Figure 3A, Supplementary Figure 3A**) suggesting a putative role in chromatin organization and gene expression regulation. To investigate the role of this lncRNA in regulating lymphoma transcription, we silenced MTAAT expression by targeting different regions – single or in combination – with gapmers technology. MTAAT expression was measured by RT-qPCR and the delivery of multiple gapmers by electroporation resulted in effective knockdown (KD) (>50%) of MTAAT across all ALK$^-$ALCL cell lines tested (**Figure 3B**). Next, we used next-generation RNA sequencing to evaluate the genome-wide transcriptional changes triggered by MTAAT silencing (MTAAT^{KD}). TLBR-2 cells were subjected to MTAAT^{KD} and RNA was collected 24h hours after. In parallel and as a control, a scrambled gapmer was also delivered. RNA-seq analysis revealed 2217 differentially expressed genes in MTAAT^{KD} compared to gapmer control. Among these, 67.5% – 1497 genes – were protein-coding. Specifically, we detected 524 downregulated and 937 upregulated genes upon lncRNA MTAAT^{KD} (FDR < 0.1) (**Figure 3C**). These findings suggest a role for MTAAT in both the activation and the repression of transcription. Notably, the genomic regions of MTAAT targets are far beyond chromosome 3 (**Figure 3D**). This suggests that MTAAT could regulate ALK$^-$ ALCL transcriptional programs *in trans* and at a genome-wide level.

Gene-set enrichment analysis revealed diverse biological processes associated with deregulated genes. Specifically, down-regulated transcripts showed significant enrichment in several gene sets related to mitochondrial respiratory chain complexes, DNA damage response, and chromatin organization. In contrast, up-regulated transcripts are mostly implicated in immune response, glycolytic process, integrated stress response as well as

regulation of mitochondrion organization (**Figure 3E**). Using RT-qPCR, we validated a representative set of upregulated genes confirming the RNA-sequencing results (Figure **3F**).

To exclude off-target effects of the gapmers designed for MTAAT^{KD}, we decided to corroborate the results by silencing MTAAT with a CRISPR-interference system, by using doxycycline-inducible dCas9-KRAB and two different single-guide RNAs (sgRNAs) targeting MTAAT promoter. Following lentiviral transduction of ALK^{-}ALCL cells, we induced dCas9-KRAB for 48 hours with doxycycline and evaluated MTAAT expression. RT-qPCR confirmed that both sgRNAs repressed the level of MTAAT by > 60% (**Supplementary Figures 3B-D)**. Importantly, the expression of 10/12 (83%) gene targets after dCas9-KRAB mediated MTAAT silencing was consistent with gapmer MTAAT^{KD}, ruling out any off-target effects (**Supplementary Figure 3E).** Collectively, the transcriptional changes that we observed upon MTAAT^{KD} indicated that this lncRNA acts as a repressor of a set of genes related to mitochondria quality control.

lncRNA MTAAT represses BNIP3 and BNIP3L via histone modifications

To understand how lncRNA MTAAT regulates the expression of mitochondria-related genes, we evaluated changes in the chromatin organization triggered upon MTAAT^{KD} investigating, by ChIP, the distribution of H3K4Me3, H3K27Ac, and RNAPII on BCL2 Interacting Protein 3 (BNIP3) and BCL2 Interacting Protein 3 Like (BNIP3L also known as NIX). These proteins resulted in target genes of lncRNA MTAAT and their loss has been implicated in the accumulation of dysfunctional mitochondria in the hematopoietic system [21,22]. After the depletion of MTAAT, H3K4Me3 and H3K27Ac levels increased significantly in BNIP3 and BNIP3L promoters (**Figures 4A-C**). Likewise, RNAPII was found to be dramatically enriched around the TSS of both genes upon MTAAT^{KD} (**Figure 4D).** Similar changes were observed in additional MTAAT target genes such as Activating Transcriptional Factor 4 (ATF4) and X-Box Binding Protein 1 (XBP1) (**Supplementary Figures 4A-D**). Concordantly with the gene

expression profile, no changes were observed in Optineurin (OPTN) gene (**Supplementary Figures 4A-E**). Furthermore, *in silico* analysis performed with catRAPID[23], showed a high interaction propensity of MTAAT with H3K27 methylation complex (**Supplementary Figure 4F)**. Collectively, these data confirm that changes in chromatin markers are directly linked to MTAAT activity on its target genes.

To strengthen the clinical relevance of MTAAT regulation on these genes, we investigated the expression of BNIP3 and BNIP3L in the retrospective cohort of ALCLs included in this study. In line with the repressive effect of MTAAT, BNIP3 expression was lower in ALK^-ALCL compared to ALK^+ALCL patients (**Figure 4E**). A similar gene expression correlation was observed in a panel of non-TCL cell lines (**Supplementary Figure 4G**). By contrast, no significant differences were observed between ALCL subtypes for BNIP3L expression (**Figure 4E**).

MTAAT sustains ALCL growth by regulating mitophagy

The transcriptional changes observed upon $MTAAT^{KD}$ are suggestive of specific disruptions in mitochondrial homeostasis, such as an aberrant increase in mitochondrial density or changes in mitochondrial morphology. We wondered if MTAAT promotes ALCL progression by controlling mitochondrial clearance. First, we asked if mitochondrial abundance changes in T-cell lymphoma upon dCas9-KRAB inducible $MTAAT^{KD}$. We evaluated mitochondrial mass by mitotracker staining and cytofluorimetric analysis. This analysis showed a time-dependent reduction in mitotracker intensity signal upon $MTAAT^{KD}$ (**Figure 5A**), whereas doxycycline treatment alone did not lead to changes (data not shown). Along the same line of evidence, we observed a strong reduction in mtDNA copy number, as determined by RT-qPCR analysis on mitochondrial gene ND1 (**Figure 5B**). Furthermore, the steady-state level of several mitochondrial proteins (Cytochrome c oxidase subunit IV -COX IV, Superoxide dismutase -SOD1, Cytochrome C -CytC, and Prohibitin 1 -PHB1) assessed by western blot,

confirmed these findings (**Figure 5C**). Since the oxidative function is strictly linked to mitochondrial network dynamics, we evaluated the mitochondrial morphology of mitotracker-stained cells using immunofluorescence. In basal condition, ALK$^-$ ALCL cells showed the mitochondrial network predominantly distributed around the perinuclear region. Upon depletion of MTAAT, mitochondria displayed a more apical/basal localization which is indicative of a less active mitochondrial state [24] (**Figure 5D**). Concordantly, mitochondrial membrane potential – evaluated by TMRM staining – was reduced upon MTAAT^{KD}, suggesting mitochondrial dysfunction **(Figure 5E).** In line with these data, ALK$^-$ALCL patients with high expression of MTAAT showed a high intensity and diffuse staining for SOD1 when compared to those expressing low levels of MTAAT **(Supplementary Figure 5A).**

Growing evidence points to a strong relationship between BNIP3 – which acts as an adaptor for tethering mitochondria to nascent autophagosomes – and the activation of a selective form of macroautophagy known as mitophagy[25]. Having observed the overexpression of BNIP3 upon MTAAT^{KD}, we asked if the observed changes in mitochondrial mass were due to the activation of mitophagy. First, we assessed if canonical mitophagy markers are detected upon MTAAT silencing. Noticeably, MTAAT^{KD} induced a time-dependent decrease of LC3 and of the autophagy receptor SQSTM1/p62 in both cell lines, suggestive of increased autophagy flux. Supporting this, the treatment with chloroquine, an autophagy inhibitor that blocks the fusion of autophagosomes with lysosomes, blocked the MTAAT-dependent increase of the autophagic flux (**Supplementary Figure 5B**). To strengthen these results**,** we sought to analyze the co-localization of specific mitophagy adaptors with the autophagosomes. We co-transfected TLBR-2 cells with plasmids encoding LC3-GFP and BNIP3-Flag and analyzed their behavior upon MTAAT^{KD}. In control cells, both markers showed diffuse and homogeneous staining across the cytoplasm (**Figure 6A**). By contrast, upon MTAAT^{KD}, both LC3 and BNIP3 accumulated into bright cytoplasmic puncta suggestive

of LC3 lipidation and BNIP3 recruitment. Importantly, LC3 and BNIP3 puncta colocalize upon MTAAT^{KD} (**Figure 6A**), indicating active mitophagy.

We hypothesized that tumor cells specifically block mitophagy to increase mitochondria mass and sustain proliferation. Therefore, we asked whether MTAAT^{KD} impacts ALK^{-}ALCL cell viability. Noticeably, growth curve analysis and viability assays showed that depleting MTAAT significantly reduces cellular proliferation in both TLBR-2 and MAC2A cell lines (**Figure 6B**). No changes were recorded in cell cycle profiles and apoptosis was not induced upon MTAAT^{KD}, consistent with energy deprivation, rather than cell death (**Supplementary Figures 5C-D**).

Altogether, our data support a model where lncRNA MTAAT exerts its function by stimulating an increase in mitochondrial mass – and energy output – that is used by ALK^{-} ALCL cells to sustain cell proliferation (**Figure 6C**).

Discussion

The implementation of digital gene expression profiling paved the way for the implementation of the transcriptomics approach in the classification of TCL, increasing the precision of diagnosis over conventional methods[26]. Progresses toward understanding the transcriptional complexity of tumors revealed how coding genes are not the only drivers of cancer progression, with non-coding transcripts – like lncRNAs – regulating essential transcriptional cascades during tumorigenesis[9,27,28]. However, how lncRNAs drive cellular and clinical phenotypes of aggressive TCL subtypes remains unknown.

In this study, we identified a set of lncRNAs that act as molecular classifiers to distinguish ALK^{+} and ALK^{-} ALCL. We also reported the role of one of these lncRNAs, which we renamed MTAAT, in regulating mitochondrial turnover and progression of aggressive ALK^{-}ALCL.

We identified MTAAT as significantly associated with ALK$^-$ ALCL phenotype in two independent cohorts of ALCL patients: first from a cohort of FFPE diagnostic biopsies analyzed by digital expression profiling with the Nanostring nCounter platform and subsequently in a cohort of frozen tissues by RT-qPCR. We also demonstrated the high accuracy of MTAAT in predicting ALK$^-$ subtypes in ALCL classification. Although the use of lncRNAs as biomarkers is still in its infancy, our results strongly suggest how digital lncRNA profiling could be integrated into diagnostic panels to improve the accuracy and precision of ALCL stratification.

We selected the lncRNAs MTAAT for functional studies based on its ALK$^-$ALCL association. Analysis of its regulatory elements showed MTAAT's intrinsic ability to regulate transcription. Transcriptional regulation by lncRNAs appears to be a mechanism widely used by hematological malignancies to control the transcription of selective pathways tuning aberrant proliferation and survival of B and T-cell [29–32].

By performing RNA-sequencing on MTAAT^{KD} cell lines, we highlighted how the transcriptional program supported by MTAAT converges on the regulation of mitochondrial pathways. Mechanistic investigations showed that the loss of MTAAT is linked to a unique phenotype characterized by an increased mitochondrial turnover through positive mitophagy stimulation, accompanied by a reduction in cell proliferation. Remarkably, lymphomas are characterized as oxidative tumors – indicating a requirement of mitochondrial function for tumor progression[33,34]. Mitochondria work as metabolic hubs to support cell growth and proliferation, and act as sensors of intracellular stresses that could threaten survival[35,36]. Although the role of mitophagy in lymphoid malignancies is still debated, some evidence indicates that the constitutive repression of autophagy/mitophagy contributes to lymphomagenesis[37–41]. The increase in the mitochondrial pool in tumor cells is also emerging as a key factor in the success of immunotherapeutic treatments[42–44], like the chimeric antigen

receptor (CAR) expressing T-cells (CAR-T) strategy[45]. CAR-T represents an incredible promise for the treatment of several malignancies and for this reason, further investigations aimed to elucidate the role of MTAAT are warranted.

Among the downstream targets of MTAAT, we identified BNIP3 whose expression is upregulated upon $MTAAT^{KD}$ via chromatin reorganization. BNIP3 was originally reported to function as a BH3-only protein that induced programmed cell death[46,47]. More recently, it has been shown to function as a stress-induced mitophagy receptor that interacts directly with LC3 to promote the turnover of otherwise healthy mitochondria [48,49]. Although various human solid cancers overexpress BNIP3 as they become hypoxic[50], its inactivation via promoter hypermethylation is a common feature of aggressive and advanced-stage cancers such as triple-negative breast cancer, hematological malignancies and advanced-stage pancreatic cancer[51–54]. In these tumors, epigenetic silencing of BNIP3 correlates with high cancer cell proliferation, poor prognostic features, and chemoresistance[55,56]. According to this finding, we found a significant reduction of BNIP3 expression in a cohort of ALK^{-}ALCL patients. This finding suggests a tumor-suppressive function of BNIP3 also in the context of ALCL. We speculate that the loss of BNIP3 associated with reduced mitophagy may create a more aggressive tumor phenotype and contribute – at least in part – to the chemoresistance observed in this malignancy. This evidence paves the way for the implementation of targeted therapeutics strategies able to re-express BNIP3 in this lymphoid malignancy.

In conclusion, we have characterized the novel lncRNA MTAAT as a new potential biomarker in ALCLs' patient stratification. Functionally, MTAAT acts as a transcriptional brake on mitophagy promoting the accumulation of mitochondria and supporting lymphoma progression. These findings corroborate our previous data showing a key role of lncRNA in the control of different transcriptional programs in ALK^{-}ALCL.

References

1. Swerdlow SH, Campo E, Pileri SA, et al. The 2016 revision of the World Health Organization classification of lymphoid neoplasms. Blood. 2016;127(20):2375-2390.

2. Ferreri AJM, Govi S, Pileri SA, Savage KJ. Anaplastic large cell lymphoma, ALK-negative. Crit Rev Oncol Hematol. 2013;85(2):206-215.

3. Parrilla Castellar ER, Jaffe ES, Said JW, et al. ALK-negative anaplastic large cell lymphoma is a genetically heterogeneous disease with widely disparate clinical outcomes. Blood. 2014;124(9):1473-1480.

4. Savage KJ, Harris NL, Vose JM, et al. ALK– anaplastic large-cell lymphoma is clinically and immunophenotypically different from both ALK+ ALCL and peripheral T-cell lymphoma, not otherwise specified: report from the International Peripheral T-Cell Lymphoma Project. Blood. 2008;111(12):5496-5504.

5. Fiore D, Cappelli LV, Broccoli A, Zinzani PL, Chan WC, Inghirami G. Peripheral T cell lymphomas: from the bench to the clinic. Nat Rev Cancer. 2020;20(6):323-342.

6. PCAWG Drivers and Functional Interpretation Working Group, PCAWG Structural Variation Working Group, PCAWG Consortium, et al. Analyses of non-coding somatic drivers in 2,658 cancer whole genomes. Nature. 2020;578(7793):102-111.

7. van Galen P. Decoding the Noncoding Cancer Genome. Cancer Discov. 2020;10(5):646-647.

8. Kapranov P, Cheng J, Dike S, et al. RNA Maps Reveal New RNA Classes and a Possible Function for Pervasive Transcription. Science. 2007;316(5830):1484-1488.

9. Statello L, Guo C-J, Chen L-L, Huarte M. Gene regulation by long non-coding RNAs and its biological functions. Nat Rev Mol Cell Biol. 2021;22(2):96-118.

10. Marchese FP, Raimondi I, Huarte M. The multidimensional mechanisms of long noncoding RNA function. Genome Biol. 2017;18(1):206.

11. Goff LA, Rinn JL. Linking RNA biology to lncRNAs. Genome Res 2015;25(10):1456-1465.

12. Ransohoff JD, Wei Y, Khavari PA. The functions and unique features of long intergenic non-coding RNA. Nat Rev Mol Cell Biol. 2018;19(3):143-157.

13. Huarte M. The emerging role of lncRNAs in cancer. Nat Med. 2015;21(11):1253-1261.

14. Anastasiadou E, Jacob LS, Slack FJ. Non-coding RNA networks in cancer. Nat Rev Cancer. 2018;18(1):5-18.

15. Iannello A, Ciarrocchi A, Fragliasso V, Vaisitti T. Lift the curtain on long non-coding RNAs in hematological malignancies: Pathogenic elements and potential targets. Cancer Lett. 2022;536:215645.

16. Fragliasso V, Verma A, Manzotti G, et al. The novel lncRNA BlackMamba controls the neoplastic phenotype of ALK– anaplastic large cell lymphoma by regulating the DNA helicase HELLS. Leukemia. 2020;34(11):2964-2980.

17. Tameni A, Sauta E, Mularoni V, et al. The DNA-helicase HELLS drives ALK– ALCL proliferation by the transcriptional control of a cytokinesis-related program. Cell Death Dis. 2021;12(1):130.

18. Fragliasso V, Chiodo Y, Ferrari-Amorotti G, et al. Phosphorylation of serine 21 modulates the proliferation inhibitory more than the differentiation inducing effects of C/EBPα in K562 cells. J Cell Biochem. 2012;113(5):1704-1713.

19. Agnelli L, Mereu E, Pellegrino E, et al. Identification of a 3-gene model as a powerful diagnostic tool for the recognition of ALK-negative anaplastic large-cell lymphoma. Blood. 2012;120(6):1274-1281.

20. Grant CE, Bailey TL, Noble WS. FIMO: scanning for occurrences of a given motif. Bioinformatics. 2011;27(7):1017-1018.

21. Sandoval H, Thiagarajan P, Dasgupta SK, et al. Essential role for Nix in autophagic maturation of erythroid cells. Nature. 2008;454(7201):232-235.

22. O'Sullivan TE, Johnson LR, Kang HH, Sun JC. BNIP3- and BNIP3L-Mediated Mitophagy Promotes the Generation of Natural Killer Cell Memory. Immunity. 2015;43(2):331-342.

23. Bellucci M, Agostini F, Masin M, Tartaglia GG. Predicting protein associations with long noncoding RNAs. Nat Methods. 2011;8(6):444-445.

24. Facucho-Oliveira JM, St. John JC. The Relationship Between Pluripotency and Mitochondrial DNA Proliferation During Early Embryo Development and Embryonic Stem Cell Differentiation. Stem Cell Rev Rep. 2009;5(2):140-158.

25. Youle RJ, Narendra DP. Mechanisms of mitophagy. Nat Rev Mol Cell Biol. 2011;12(1):9-14.

26. Amador C, Bouska A, Wright G, et al. Gene Expression Signatures for the Accurate Diagnosis of Peripheral T-Cell Lymphoma Entities in the Routine Clinical Practice. J Clin Oncol. 2022;40(36):4261-4275.

27. Palazzo AF, Koonin EV. Functional Long Non-coding RNAs Evolve from Junk Transcripts. Cell. 2020;183(5):1151-1161.

28. Schmitt AM, Chang HY. Long Noncoding RNAs in Cancer Pathways. Cancer Cell. 2016;29(4):452-463.

29. Doose G, Haake A, Bernhart SH, et al. MINCR is a MYC-induced lncRNA able to modulate MYC's transcriptional network in Burkitt lymphoma cells. Proc Natl Acad Sci U S A. 2015;112(38):E5261-5270.

30. Zhao P, Ji M-M, Fang Y, et al. A novel lncRNA TCLlnc1 promotes peripheral T cell lymphoma progression through acting as a modular scaffold of HNRNPD and YBX1 complexes. Cell Death Dis. 2021;12(4):321.

31. Zhao C-C, Jiao Y, Zhang Y-Y, et al. Lnc SMAD5-AS1 as ceRNA inhibit proliferation of diffuse large B cell lymphoma via Wnt/β-catenin pathway by sponging miR-135b-5p to elevate expression of APC. Cell Death Dis. 2019;10(4):252.

32. Cui Y, Xu H, Yang Y, et al. The regulation of miR-320a/XBP1 axis through LINC00963 for endoplasmic reticulum stress and autophagy in diffuse large B-cell lymphoma. Cancer Cell Int. 2021;21(1):305.

33. Li M, Teater MR, Hong JY, et al. Translational Activation of ATF4 through Mitochondrial Anaplerotic Metabolic Pathways Is Required for DLBCL Growth and Survival. Blood Cancer Discov. 2022;3(1):50-65.

34. Bhalla K, Jaber S, Nahid MN, et al. Role of hypoxia in Diffuse Large B-cell Lymphoma: Metabolic repression and selective translation of HK2 facilitates development of DLBCL. Sci Rep. 2018;8(1):744.

35. Giacomello M, Pyakurel A, Glytsou C, Scorrano L. The cell biology of mitochondrial membrane dynamics. Nat Rev Mol Cell Biol. 2020;21(4):204-224.

36. Eisner V, Picard M, Hajnóczky G. Mitochondrial dynamics in adaptive and maladaptive cellular stress responses. Nat Cell Biol. 2018;20(7):755-765.

37. Bertolo C, Roa S, Sagardoy A, et al. *LITAF* , a BCL6 target gene, regulates autophagy in mature B-cell lymphomas. Br J Haematol. 2013;162(5):621-630.

38. Wang Z, Xu F, Yuan N, et al. Rapamycin inhibits pre-B acute lymphoblastic leukemia cells by downregulating DNA and RNA polymerases. Leuk Res. 2014;38(8):940-947.

39. Cheng C, Wang T, Song Z, et al. Induction of autophagy and autophagy-dependent apoptosis in diffuse large B-cell lymphoma by a new antimalarial artemisinin derivative, SM1044. Cancer Med. 2018;7(2):380-396.

40. Nahimana A, Attinger A, Aubry D, et al. The NAD biosynthesis inhibitor APO866 has potent antitumor activity against hematologic malignancies. Blood. 2009;113(14):3276-3286.

41. Torossian A, Broin N, Frentzel J, et al. Blockade of crizotinib-induced BCL2 elevation in ALK-positive anaplastic large cell lymphoma triggers autophagy associated with cell death. Haematologica. 2019;104(7):1428-1439.

42. Sainero-Alcolado L, Liaño-Pons J, Ruiz-Pérez MV, Arsenian-Henriksson M. Targeting mitochondrial metabolism for precision medicine in cancer. Cell Death Differ. 2022;29(7):1304-1317.

43. Missiroli S, Perrone M, Genovese I, Pinton P, Giorgi C. Cancer metabolism and mitochondria: Finding novel mechanisms to fight tumours. eBioMedicine 2020;59:102943.

44. Porporato PE, Filigheddu N, Pedro JMB-S, Kroemer G, Galluzzi L. Mitochondrial metabolism and cancer. Cell Res. 2018;28(3):265-280.

45. Zhang L, Zhang W, Li Z, et al. Mitochondria dysfunction in CD8+ T cells as an important contributing factor for cancer development and a potential target for cancer treatment: a review. J Exp Clin Cancer Res. 2022;41(1):227.

46. Chen G, Ray R, Dubik D, et al. The E1B 19K/Bcl-2–binding Protein Nip3 is a Dimeric Mitochondrial Protein that Activates Apoptosis. J Exp Med. 1997;186(12):1975-1983.

47. Ray R, Chen G, Vande Velde C, et al. BNIP3 Heterodimerizes with Bcl-2/Bcl-XL and Induces Cell Death Independent of a Bcl-2 Homology 3 (BH3) Domain at Both Mitochondrial and Nonmitochondrial Sites. J Biol Chem. 2000;275(2):1439-1448.

48. Hanna RA, Quinsay MN, Orogo AM, Giang K, Rikka S, Gustafsson ÅB. Microtubule-associated Protein 1 Light Chain 3 (LC3) Interacts with Bnip3 Protein to Selectively Remove Endoplasmic Reticulum and Mitochondria via Autophagy. J Biol Chem. 2012;287(23):19094-19104.

49. Glick D, Zhang W, Beaton M, et al. BNip3 Regulates Mitochondrial Function and Lipid Metabolism in the Liver. Mol Cell Biol. 2012;32(13):2570-2584.

50. Sowter HM, Ferguson M, Pym C, et al. Expression of the cell death genes BNip3 and NIX in ductal carcinomain situ of the breast; correlation of BNip3 levels with necrosis and grade. J Pathol. 2003;201(4):573-580.

51. Chourasia AH, Tracy K, Frankenberger C, et al. Mitophagy defects arising from BNip3 loss promote mammary tumor progression to metastasis. EMBO Rep. 2015;16(9):1145-1163.

52. Koop EA, van Laar T, van Wichen DF, de Weger RA, Wall E van der, van Diest PJ. Expression of BNIP3 in invasive breast cancer: correlations with the hypoxic response and clinicopathological features. BMC Cancer. 2009;9(1):175.

53. Murai M, Toyota M, Satoh A, et al. Aberrant DNA methylation associated with silencing BNIP3 gene expression in haematopoietic tumours. Br J Cancer. 2005;92(6):1165-1172.

54. Okami J, Simeone DM, Logsdon CD. Silencing of the Hypoxia-Inducible Cell Death Protein BNIP3 in Pancreatic Cancer. Cancer Res. 2004;64(15):5338-5346.

55. Akada M, Crnogorac-Jurcevic T, Lattimore S, et al. Intrinsic Chemoresistance to Gemcitabine Is Associated with Decreased Expression of BNIP3 in Pancreatic Cancer. Clin Cancer Res. 2005;11(8):3094-3101.

56. Erkan M, Kleeff J, Esposito I, et al. Loss of BNIP3 expression is a late event in pancreatic cancer contributing to chemoresistance and worsened prognosis. Oncogene. 2005;24(27):4421-4432.

Figure Legends

Figure 1. XLOC_211989 stratifies ALK$^-$ ALCL patients

(**A**) Outline of the study workflow for the FFPE training cohort to classify ALCL patients based on transcriptomic profiles. Created with BioRender.com. (**B**) Principal component analysis (PCA) shows the variance between ALK$^+$ ALCL (red dots) and ALK$^-$ ALCL (grey dots) samples of the FFPE training cohort explained by the expression level of the 17 lncRNAs. (**C**) Dot plots show gene expression counts distribution of the 11 statistically significant lncRNAs among ALK$^+$ ALCL (red dots) and ALK$^-$ ALCL (black dots) of the FFPE training cohort. Comparisons were considered significant for $p \leq 0.05$ (*). (**D**) The alluvial plot shows the workflow for the identification and validation of XLOC_211989. (**E**) Boxplot representing the expression of XLOC_211989 among ALK$^+$ (red) and ALK$^-$ (grey) ALCL evaluated by RT-qPCR in the validation cohort. The comparison was considered significant for $p \leq 0.05$ (*). (**F**) Correlation plot between ALK and XLOC_211989 normalized and log2 transformed gene counts in the FFPE training cohort (left panel). Correlation plot between BlackMamba and XLOC_211989 normalized and log2 transformed gene counts training cohort (right panel). (**G**) ROC curve showing the performance of XLOC_211989-based scoring system in the training cohort of ALCL patients. The curve is colored according to XLOC_211989 adjusted values, the relation between colors and different values is represented by the bar on the right. The formula has been generated by the generalized linear regression model.

Figure 2. MTAAT is a novel lncRNA

(**A**) Schematic representation of locus and structure of MTAAT showing the position and enrichment level of active marks of transcription assessed by ChIP-seq in TLBR-2 cells. ChIP-RT-qPCR detection of RNAPII (**B**), H3K4me3 (**C**), and H3K27Ac (**D**) markers on MTAAT fragments in ALK$^-$ALCL cell lines. GAPDH promoter was used as CTR+ whereas a non-coding intergenic region (CTR−) served as a negative control. The values are

representative of three independent experiments. (**E**) Luciferase activity of MTAAT-fragment into pGL3 vector. Data are represented as a normalized ratio of firefly-Renilla luciferase activities and are expressed as mean values ± SD (*n* = 3). ***p*≤0.01. (**F**) Graphs show the most representative enriched TFs-related pathways. For each pathway, the TF with the major number of interactions was colored in yellow. These graphs were created using cytoskape software.

Figure 3. MTAAT KD results in transcriptional changes

(**A**) Relative expression of MTAAT in cytoplasm, nucleus, and chromatin fraction of ALK-ALCL cell lines (average of three independent experiments ± S.D.). One-tailed-t-test. **, p ≤ 0.01. (**B**) RT-qPCR analysis of MTAAT expression 24 hours after gapmers nucleofection in MAC2A and TLBR-2 cells. One-tailed-t-test. **, p ≤ 0.01. (**C**) The heatmap depicts hierarchical clustering based on 2217 differentially expressed genes, whose read counts are Z-score normalized. Unsupervised hierarchical clustering was performed between gapmer control and gapmers #1+#2 samples (as indicated by the colored bar on columns) with a complete linkage method. Color intensity for each gene shows Z-score values ranging from red for upregulation to green for downregulation (left panel). The graph shows the number and the category of deregulated genes after RNA-seq in TLBR-2 nucleofected with gapmers #1+#2 compared to gapmer control. (**D**) The circular plot displays the genomic location of MTAAT (highlighted with a red line) and the protein-coding genes differentially expressed upon its knockdown. Red links connect lncRNA MTAAT to upregulated genes, green links connect lncRNA MTAAT to downregulated genes (right panel). (**E**) Most significant enriched pathways (adjusted p-value<0.05) are represented showing the up and the down-regulated number of DE genes mapped in each considered pathway (left panel). The heatmap depicts validated significantly downregulated genes. The orange-red color bar shows the fold difference on the Log_2 scale calculated between DOX and CTR samples. Lighter orange

represents the most downregulated genes (right panel). (**F**) RT-qPCR validation of significantly upregulated genes obtained from RNA-sequencing in TLBR-2 cells after nucleofection with gapmers (24 hours). Each data represents the mean ± SEM (*n* = 3). Two-tailed *t*-test. **p*<0.05; ***p*<0.01.

Figure 4. **MTAAT KD modifies active transcriptional markers on regulatory elements of its gene targets**

(**A**) Graphs show the TSS and fragments around the TSS of BNIP3 and BNIP3L. ChIP-qPCR detection of H3K4me3 (**B**), H3K27Ac (**C**), and RNAPII (**D**) on MTAAT-genes target fragments in TLBR-2 $MTAAT^{KD}$ cell lines. The values are representative of three independent experiments. (**E**) Box plots show the expression level of BNIP3 and BNIP3L in the FFPE-ALCL cohort. One-tailed-t-test. *, p ≤ 0.01

Figure 5. **MTAAT inactivation impairs mitochondria homeostasis.**

(**A**) Histograms of FACS analysis show a left shift of mitotracker red fluorescence in $MTAAT^{KD}$ cell lines (red and yellow) compared to control (grey) at 48 and 72 hours after doxycycline treatment. Bar plots show the mean fluorescence intensity (MFI) of cells stained with mitotracker-red and analyzed by FACS. Each data represents the mean ± SEM (n= 3). Two-tailed *t*-test. **p*<0.05; ***p*<0.01 relative to CTR. (**B**) Copy number analysis of mitochondrial gene ND1 normalized on nuclear gene β-actin (48 and 72 hours after doxycycline treatment). Each data represents the mean ± SEM (n= 3). Two-tailed *t*-test. **p*<0.05; ***p*<0.01 relative to CTR. (**C**) Western blots show the expression of a set of mitochondrial proteins after MTAAT KD in TLBR-2 and MAC2A cells (72 hours). (**D**) Immunofluorescences show the localization of mitochondria in $MTAAT^{KD}$ cells. Cells were stained with mitotracker-red dye and DAPI. The white scale bar represents 10 µm. Relative bar plots indicate the percentage of mitotracker-red stained cells with apical/basal

mitochondria (n=500 cells). Each data represents the mean ± SEM (n= 3). Two-tailed *t*-test. **p*<0.05; ***p*<0.01 relative to CTR. (**E**) Histograms of FACS analysis show a right shift of TMRM fluorescence in MTAAT^{KD} cell lines (red and yellow) compared to the control (grey). Bar plots show the mean fluorescence intensity (MFI) of cells stained with TMRM and analyzed by FACS. Each data represents the mean ± SEM (n= 3). Two-tailed *t*-test. **p*<0.05; ***p*<0.01 relative to CTR.

Figure 6. **MTAAT KD promotes mitophagy and reduces cellular proliferation**

(**A**) Immunofluorescence images of TLBR-2 MTAAT^{KD} cells after 48 h of doxycycline (DOX) induction. Cells were stained with DAPI and FLAG antibodies for BNIP3 detection. The white scale bar represents 10 µm. (**B**) Growth curves show the proliferation of cells after MTAAT depletion. Each data represents the mean ± SEM (n= 3). Two-tailed *t*-test. ***p*<0.01 relative to CTR. (**C**) Graphical model of MTAAT function in lymphoma. Created with BioRender.com

Figure 1

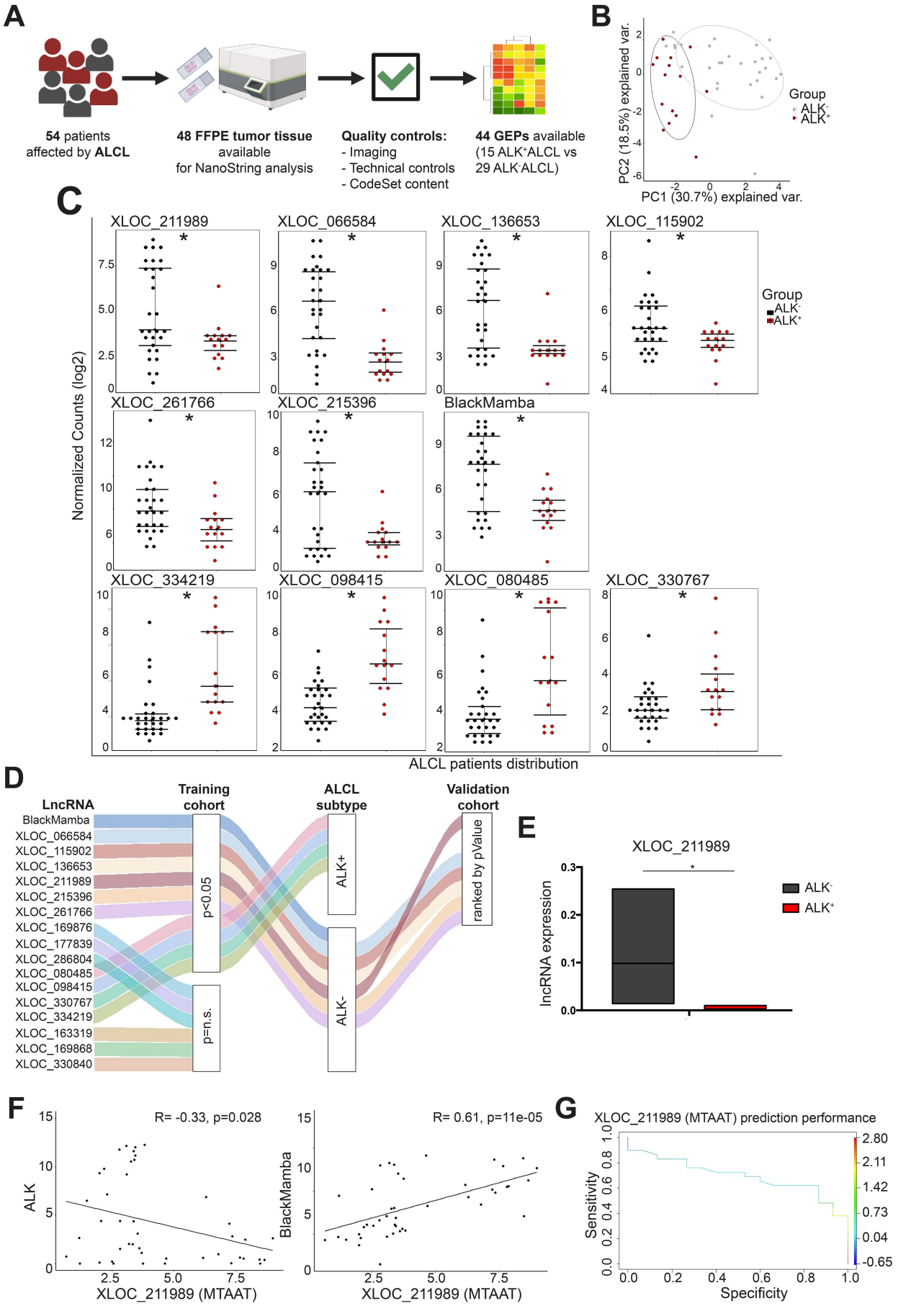
A
54 patients affected by ALCL
48 FFPE tumor tissue available for NanoString analysis
Quality controls:
- Imaging
- Technical controls
- CodeSet content
44 GEPs available (15 ALK+ALCL vs 29 ALK-ALCL)
B
PC2 (18.5%) explained var.
PC1 (30.7%) explained var.
Group
ALK-
ALK+
C
XLOC_211989
XLOC_066584
XLOC_136653
XLOC_115902
XLOC_261766
XLOC_215396
BlackMamba
XLOC_334219
XLOC_098415
XLOC_080485
XLOC_330767
Normalized Counts (log2)
ALCL patients distribution
D
LncRNA
Training cohort
ALCL subtype
Validation cohort
BlackMamba
XLOC_066584
XLOC_115902
XLOC_136653
XLOC_211989
XLOC_215396
XLOC_261766
XLOC_169876
XLOC_177839
XLOC_286804
XLOC_080485
XLOC_098415
XLOC_330767
XLOC_334219
XLOC_163319
XLOC_169868
XLOC_330840
p<0.05
p=n.s.
ALK+
ALK-
ranked by pValue
E
XLOC_211989
lncRNA expression
ALK-
ALK+
F
R= -0.33, p=0.028
ALK
XLOC_211989 (MTAAT)
R= 0.61, p=11e-05
BlackMamba
XLOC_211989 (MTAAT)
G
XLOC_211989 (MTAAT) prediction performance
Sensitivity
Specificity

Figure 2

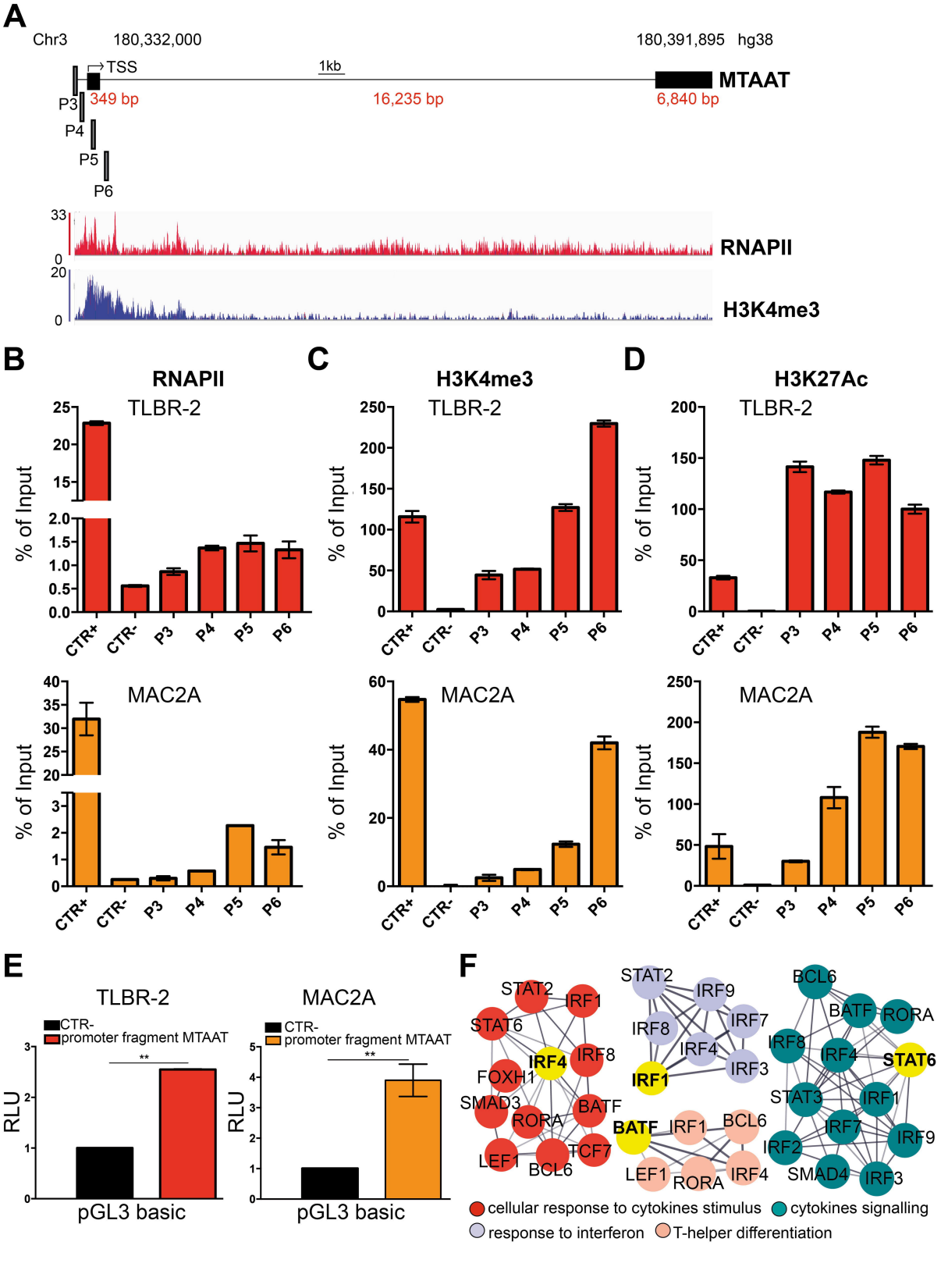
A
Chr3
180,332,000
180,391,895
hg38
TSS
1kb
MTAAT
P3
P4
P5
P6
349 bp
16,235 bp
6,840 bp
RNAPII
H3K4me3
B
RNAPII
TLBR-2
MAC2A
% of Input
C
H3K4me3
TLBR-2
MAC2A
% of Input
D
H3K27Ac
TLBR-2
MAC2A
% of Input
CTR+
CTR-
P3
P4
P5
P6
E
TLBR-2
MAC2A
CTR-
promoter fragment MTAAT
RLU
pGL3 basic
F
STAT2
IRF1
STAT6
IRF4
IRF8
FOXH1
SMAD3
BATF
RORA
LEF1
TCF7
BCL6
IRF9
IRF7
IRF3
BCL6
BATF
RORA
STAT3
IRF2
SMAD4
cellular response to cytokines stimulus
cytokines signalling
response to interferon
T-helper differentiation

Figure 3

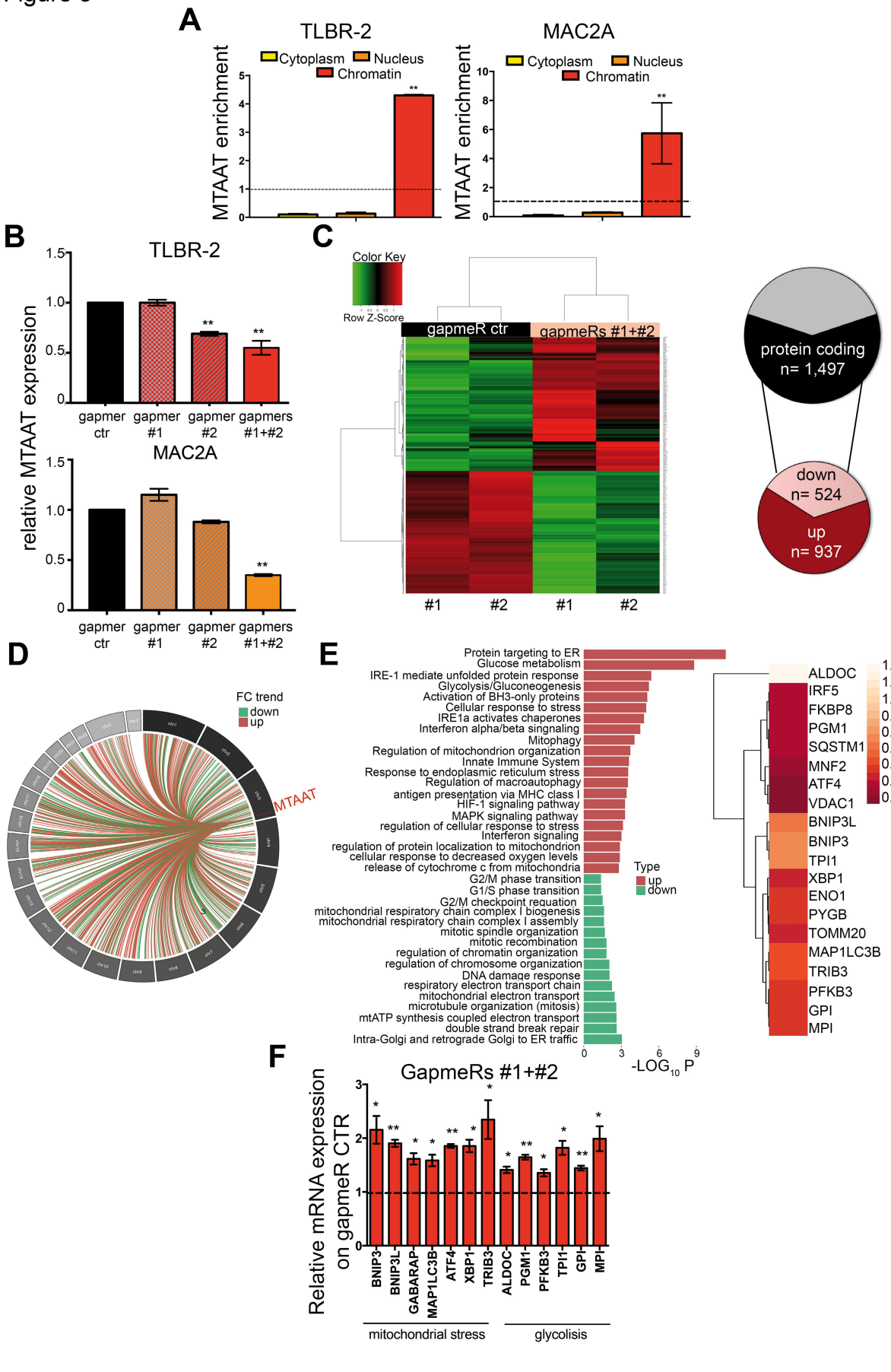
A
TLBR-2
MAC2A
Cytoplasm
Nucleus
Chromatin
MTAAT enrichment
B
TLBR-2
MAC2A
relative MTAAT expression
gapmer ctr
gapmer #1
gapmer #2
gapmers #1+#2
C
Color Key
Row Z-Score
gapmeR ctr
gapmeRs #1+#2
protein coding n= 1,497
down n= 524
up n= 937
D
FC trend
down
up
MTAAT
E
Protein targeting to ER
Glucose metabolism
IRE-1 mediate unfolded protein response
Glycolysis/Gluconeogenesis
Activation of BH3-only proteins
Cellular response to stress
IRE1a activates chaperones
Interferon alpha/beta singnaling
Mitophagy
Regulation of mitochondrion organization
Innate Immune System
Response to endoplasmic reticulum stress
Regulation of macroautophagy
antigen presentation via MHC class I
HIF-1 signaling pathway
MAPK signaling pathway
regulation of cellular response to stress
Interferon signaling
regulation of protein localization to mitochondrion
cellular response to decreased oxygen levels
release of cytochrome c from mitochondria
G2/M phase transition
G1/S phase transition
G2/M checkpoint requation
mitochondrial respiratory chain complex I biogenesis
mitochondrial respiratory chain complex I assembly
mitotic spindle organization
mitotic recombination
regulation of chromatin organization
regulation of chromosome organization
DNA damage response
respiratory electron transport chain
mitochondrial electron transport
microtubule organization (mitosis)
mtATP synthesis coupled electron transport
double strand break repair
Intra-Golgi and retrograde Golgi to ER traffic
Type
up
down
-LOG10 P
ALDOC
IRF5
FKBP8
PGM1
SQSTM1
MNF2
ATF4
VDAC1
BNIP3L
BNIP3
TPI1
XBP1
ENO1
PYGB
TOMM20
MAP1LC3B
TRIB3
PFKB3
GPI
MPI
F
GapmeRs #1+#2
Relative mRNA expression on gapmeR CTR
BNIP3
BNIP3L
GABARAP
MAP1LC3B
ATF4
XBP1
TRIB3
ALDOC
PGM1
PFKB3
TPI1
GPI
MPI
mitochondrial stress
glycolisis

Figure 4

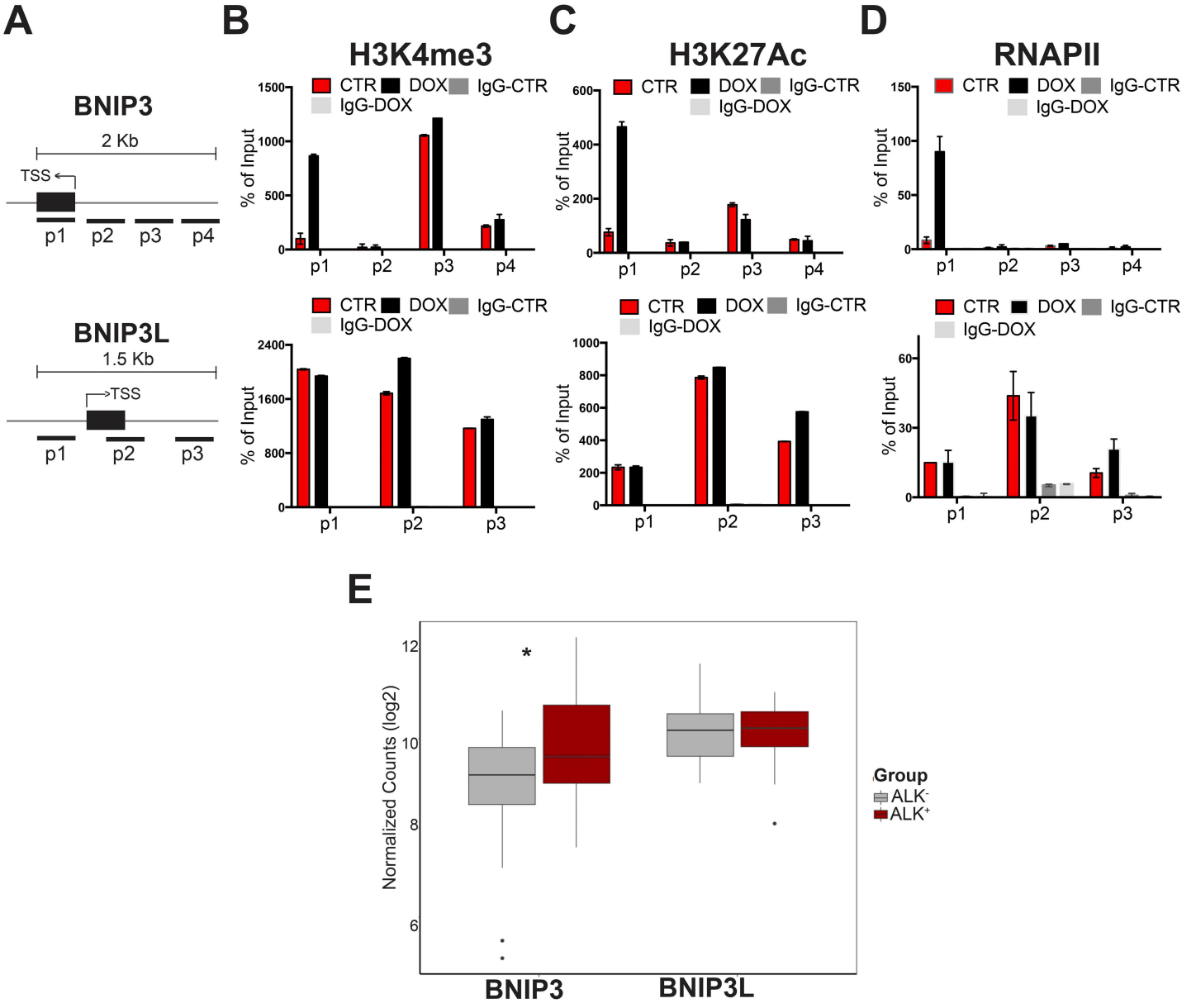
A
BNIP3
2 Kb
TSS
p1
p2
p3
p4
BNIP3L
1.5 Kb
TSS
p1
p2
p3
B
H3K4me3
CTR
DOX
IgG-CTR
IgG-DOX
% of Input
C
H3K27Ac
D
RNAPII
E
Normalized Counts (log2)
Group
ALK-
ALK+
BNIP3
BNIP3L

Figure 5

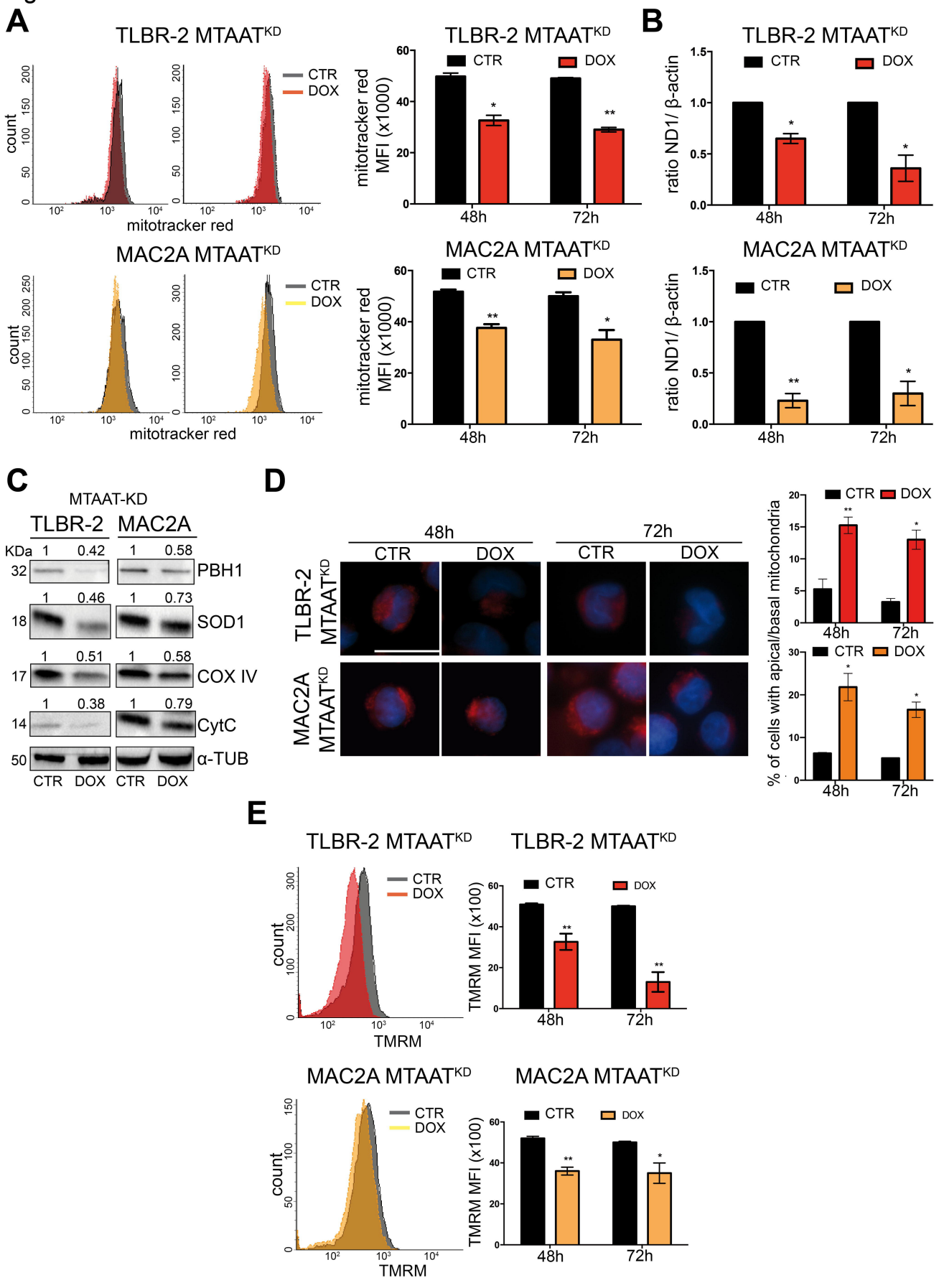
A
TLBR-2 MTAAT^KD
CTR
DOX
count
mitotracker red
TLBR-2 MTAAT^KD
mitotracker red MFI (x1000)
48h
72h
MAC2A MTAAT^KD
MAC2A MTAAT^KD
B
TLBR-2 MTAAT^KD
ratio ND1/ β-actin
MAC2A MTAAT^KD
C
MTAAT-KD
TLBR-2
MAC2A
KDa
PBH1
SOD1
COX IV
CytC
α-TUB
D
48h
72h
TLBR-2 MTAAT^KD
MAC2A MTAAT^KD
% of cells with apical/basal mitochondria
E
TLBR-2 MTAAT^KD
TMRM
TMRM MFI (x100)
MAC2A MTAAT^KD

Figure 6

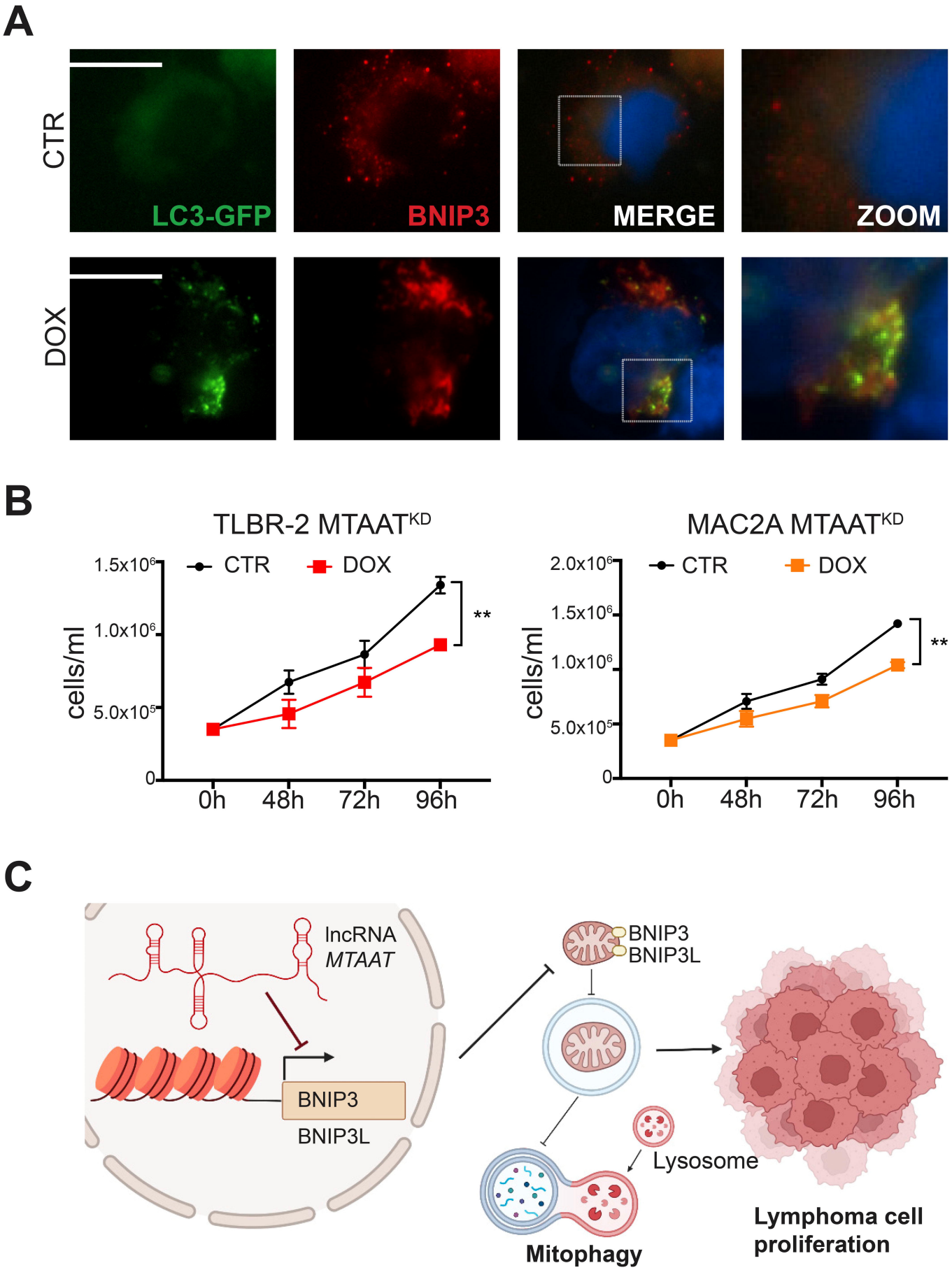
A
CTR
DOX
LC3-GFP
BNIP3
MERGE
ZOOM
B
TLBR-2 MTAAT^KD
MAC2A MTAAT^KD
CTR
DOX
cells/ml
1.5x10^6
1.0x10^6
5.0x10^5
0
2.0x10^6
0h
48h
72h
96h
**
C
lncRNA
MTAAT
BNIP3
BNIP3L
Lysosome
Mitophagy
Lymphoma cell
proliferation

Long non-coding RNA mitophagy and ALK$^-$ anaplastic lymphoma associated transcript: a novel regulator of mitophagy in T cell Lymphoma

Supplementary Methods

Cell culture and treatments

The human ALK$^-$ and ALK$^+$ALCL cell lines MAC2A, FePD, L82, SUPM2, SUDHL1, and KARPAS299 were a kind gift of Dr. Giorgio Inghirami. The human Breast Implanted Associated (BIA)-ALCL cell lines TLBR-2 and TLBR-3 were a kind gift of Dr. Alain Epstein. The human CUTLL1 were a kind gift from Dr. Iannis Aifantis while human K562, MJ, and KCL22 cell lines were a kind gift from Dr. Bruno Calabretta. The human cell lines TPC1, BCPAP, 8505, CAL62, H1299, H1975, H1650, MB231, OCI-LY10, OCI-LY13 and NUDUL1 were a kind gift of Dr. Ciarrocchi. Cell identity was determined yearly. All cell lines were genotyped and routinely tested for Mycoplasma contamination. Cell lines were cultured in RPMI-1640 medium (Gibco) supplemented with 10% FBS at 37 °C in an atmosphere of 5% CO_2. TLBR-2 cells were supplemented with IL2 (20U/ml). Doxycycline hyclate was purchased from Sigma and dissolved in H_2O.

Chloroquine was purchased from Sigma and dissolved in H_2O.

Cytoplasm/Nucleus fractionation

ALCL cells were resuspended in hypotonic buffer (20mM tris-HCl pH 7; 10mM NaCl; 3mN MgCl2; 0.3% NP40) supplemented with SUPERase•In (Ambion) for 15 min on ice. After a centrifugation at 800*g* for 10 min, the supernatant was collected as the cytoplasmic fraction. The pellet was resuspended in cell extraction buffer (10mM Tris pH 7.4; 2mM Na3VO4; 100mM NaCl; 1% Triton-x100; 1mM EDTA; 10% glycerol; 1mM EGTA; 0.1% SDS; 1mM NaF; 0.5% Na-deoxycholate; 20mM Na4P2O7) supplemented with RNase inhibitors for 30 min on ice. After a centrifugation at 14,000*g* for 30 min, the supernatant was collected as the nuclear

fraction. Chromatin was pelleted at maximum speed for 3 min. All fractions were resuspended in TRIzol (Invitrogen) and RNA was extracted following the standard protocol. All fractions were resuspended in TRIzol (Invitrogen) and RNA was extracted following the standard protocol.

Generation of TLBR-2 and MAC2A dCas9-KRAB MTAAT^{KD} cell lines

pHAGE TRE dCas9-KRAB was a gift from Rene Maehr & Scot Wolfe (Addgene plasmid # 50917; http://n2t.net/addgene:50917; RRID:Addgene_50917). Vector was packaged into lentiviral particles HEK 293T-cell line and used for infection of low passages MAC2A or TLBR-2. Cells were selected with 0.5 mg/ml of Geneticin™ Selective Antibiotic (G418 Sulfate, Gibco), for 3 days (both MAC2A and TLBR-2).

Annealed sgRNA oligomers were ligated into BsmB1 digested LRG2.1 plasmid (a gift from Christopher Vakoc, addgene plasmid #108098; http://n2t.net/addgene:108098; RRID:Addgene_108098) and lentiviral particles were created as previously described[16]. Viral particles were used to infect TLBR-2 dCas9-KRAB and MAC2A dCas9-KRAB previously derived cell lines. Infected cells were then purified by gating GFP+ cells using BD FACS Melody cell sorter. The list of sgRNA sequences is provided in **supplementary table 2**.

Gene Expression Profiling (GEP) by Nanostring

Total RNA was extracted by Maxwell® RSC RNA FFPE kit (Promega) starting from 5 slides of 5μm FFPE tissue. RNA quantity and quality were assessed by NanoDrop2000 (Thermo Fisher Scientific). For samples that reached the quality standards (A260/A280 ≥ 1.7 and A260/A230 ≥ 1.8), we evaluated the gene expression profile (GEP) by nCounter platform (NanoString Technologies) using a custom panel. This panel includes a total of 39 transcripts: 17/18 lncRNAs from the non coding-signature previously generated by RNA-seq platform[16], that showed a suitable sequence to generate unique and specific nCounter

probes, 4 ALCL-restricted coding transcripts (ALK, TMOD1, BATF, TNFRSF8), 1 ALCL-specific non-coding transcript (ERBB4)[20], BNIP3, BNIP3L and 15 housekeeping (**supplementary table 3**). Analysis of detected gene counts was performed by nSolver Analysis Software 4.0 (NanoString Technologies) as previously described[21]. Briefly, for samples that passed imaging quality controls, raw counts of coding genes were subjected to background subtraction as mean counts of negative controls plus two standard deviation and then normalized on synthetic positive controls. On the contrary, no background subtraction was applied to non coding transcript that were normalized on synthetic positive controls only. After that, counts normalized on technical controls were further normalized on the 3 housekeeping genes with the lowest coefficient of variation (COG7, DNAJC14, ERCC3) and log2 transformed. Applying the *3 gene model*[22] and considering the lack of ALK expression, 29 patients were classified as ALK- ALCL. Almost all these patients (n=26, 90%) showed the expression of at least one among TMOD, BATF and TNFRSF8 genes **(supplementary table 4).** On the contrary, 14 patients were classified as ALK^+ ALCL because of high ALK expression. This group included 3 ALK^- ALCL that were re-classified as ALK+ because of their high level of ALK mRNA. Moreover, one patient that showed a low level of both ALK and 3 genes model was classified as ALK^+ ALCL according to the current WHO diagnostic criteria classification [1].

Positive expression of the genes included in the 3 genes model (TMOD, BATF and TNFRSF8) was considered for level of expression over the 1^{st} quartile of normalized gene counts distribution.

To investigate lncRNAs differential expression a build ratio analysis was performed by comparing the transcriptomic profiles of ALK^- and ALK^+ samples. For each comparison, the p-value was calculated as Kruskal-Wallis test since data were not normal distributed. Correlation between normalized gene counts was evaluated by Pearson correlation coefficient. ERBB4, was used as positive technical control for lncRNA detection.

To evaluate the performance of MTAAT in predicting ALCL subtypes, we constructed the receiver operating characteristic (ROC) curve and calculated the area under the ROC curve (AUC) and the relative accuracy of prediction. Bioinformatic analyses on GEP were conducted by R Software v4.1.3 using the following R packages: ggplot2, ggbiplot (function prcomp), corrplot, pROC and ROCR.

Chromatin immunoprecipitation (ChIP) and ChIP-sequencing

TLBR-2 cells ($15*10^6$/IP) were crosslinked for 15 min with 1% formaldehyde, lysed and sonicated for 15 cycles (30 min ON, 30 min OFF) using Bioruptor Pico Sonicator (Diagenode, Denville, NJ, USA) to obtain 100-200 bp chromatin fragments. Chromatin was precipitated overnight using Dynabeads Protein G magnetic beads (Thermo Fisher Scientific) and 1,5ug of H3K4me3 (Rabbit Polyclonal, Abcam), 1,5ug of H3K27Ac (ab4729, Rabbit Polyclonal, Abcam), 2,5ug of RNAPII (Rabbit Monoclonal, #14958, Cell Signaling Technology), or IgG-isotype control (#66362, Cell Signaling Technology). A fraction equal to 0.25% of total chromatin was used as input. For Chip, each RT-qPCR value was normalized over the appropriate input control and reported in graphs as a % of input. The list of primers used is provided in **supplementary table 1**.

For ChIP-seq, samples were quantified with Qubit (Thermo Fisher Scientific), and the quality was evaluated by Bioanalyzer (Agilent Technologies). Library for sequencing was obtained following the NEBNext Ultra II DNA Library Prep Kit for Illumina (New England BioLabs, Ipswich, MA, USA) using 3-10 ng ChIP DNA as starting material. Triplicates were sequenced on Illumina NextSeq500 high-output cartridge (single stranded, reads length 75 bp-1 × 75).

Library preparation and RNA-sequencing

RNA-seq libraries were obtained starting from 100 ng of total RNA following Illumina Stranded TotalRNA Prep Ligation with Ribo-zero Plus protocol. Sequencing was performed using Illumina NEXTSeq high-output cartridge (double-stranded, reads length 75bp-2 ×75).

Sequencing data processing

Sequencing data quality was assessed using the FastQC v0.11.8 software (www.bioinformatics.babraham.ac.uk/projects/fastqc/), low quality reads were discarded, and where residual adapters were present, they were removed using Trimmomatic (v.0.39) software.

For ChIP-seq, filtered reads were aligned to the human reference genome (GRCh38/hg38 assembly) by using Bowtie2 version 2.3.5.1. Picard tool (http://broadinstitute.github.io/picard) and samtools 1.9v (http://samtools.sourceforge.net/) were used to remove duplicates and unmapped reads and to retain uniquely aligned reads for downstream analyses. Peak calling was performed using MACS2 (v.2.1.3.3). Significant peaks ($q < 0.05$) were merged, and high confidence peaks enriched in at least 2 of 3 replicates were retained for the analysis.

ChIPseeker R package was used for assigning peaks to the nearest genes, according to GRCh38/hg38 annotation, using a transcription start site (TSS) window of ±3 kb.

For RNA-seq, filtered paired-end reads were aligned to the human reference transcriptome (GRCh38, Gencode release 30 using STAR version 2.7), and gene abundances were estimated with RSEM algorithm (v1.3.1). Differential analysis was performed with R package DESeq2, considering a false discovery rate (FDR) of 10% and excluding genes with low read counts. Significantly deregulated genes underwent enrichment analysis, performed through enrichR package on Gene Ontology biological processes using a significance threshold of 0.05 on P value adjusted for multiple testing using the Benjamini–Hochberg correction.

Prediction of TF binding sites

TFs binding sites prediction was performed applying FIMO algorithm on a selected region of 500bp around MTAAT TSS. HOCOMOCO and JASPAR were used as reference motifs databases and q-value <0.1 was considered for significant motif enrichment.

Western blot

Western blot analysis was performed using standard techniques. The primary antibodies were: Caspase-3 (#9662, Rabbit Monoclonal, Cell Signaling Technology), PARP-1 (ab137653, Rabbit Polyclonal, Abcam), p62/SQSTM (ab91526, Rabbit Polyclonal, Abcam), LC3 A/B (#4108, Rabbit Monoclonal, Cell Signaling Technology), HA (C29FA, Rabbit, Cell Signaling Technology), B-Actin (AC-15, Mouse, Sigma-Aldrich). All secondary antibodies (rabbit and mouse) were HRPconjugated (GE Healthcare) and diluted 1:3000. Densitometric analysis was performed using ImageJ software.

Cell cycle analysis

For cell cycle analysis, the hypotonic propidium iodide (PI) method was used. All flow cytometry analyses were performed with FACSCanto™ II Cell Analyzer (BD Biosciences).

Generation of promoter and enhancer plasmids

pGL3 basic and pGL3 promoter plasmids (Promega) with the selected putative promoter/enhancer region of MTAAT were generated as follow: the selected region was amplified by PCR from genomic DNA of TLBR-2 using PhusionTM Plus DNA Polymerase kit (Thermo Fisher Scientific) with an upstream oligomer containing a 5′-KpnI site and a downstream oligomer containing a 3′-XhoI site (**supplementary table1**). PCR product of the right length was isolated from a 1% agarose gel, purified, and finally cloned into KpnI-XhoI-digested pGL3 basic/ pGL3 promoter vectors. The plasmids were sequenced and checked for right sequence.

Plasmid transfection

p3XFlagCMV10_BNIP3 was obtained cloning the gBlock Gene Fragment (IDT) for BNIP3 into the p3XflagCMV10 (Sigma Aldrich). For EGFP-LC3 expression, gBlock Gene Fragment (Integrated DNA Technologies, IDT) for LC3 was cloned into the pEGFP-C3 (Diatech Lab Line). 48 hours after induction with doxycycline, cells were nucleofected with a total of 400ng of plasmids and the co-localization of the two proteins was evaluated by immunofluorescence 24 hours after nucleofection.

Luciferase Assay

MAC2A and TLBR-2 cells (1 × 10^6) were transfected with 400 ng of reporter pGL3-luciferase plasmids using the Cell Line Nucleofector Kit SF and 4D Amaxa Nucleofector (program FI115 for MAC2A, DS-130 for TLBR-2). Twenty-four hours after transfection, cells were harvested, and luciferase activity was measured using the Dual-Luciferase Reporter Assay System (Promega) in a GloMax Discover Luminometer (Promega) according to the manufacturer's instructions. For each sample, firefly luciferase activity was normalized on *Renilla* luciferase activity and transactivation of the various reporter constructs was expressed as fold induction on empty vector (pGL3-basic or pGL3-promoter) activity.

Immunohistochemistry (IHC)

Formalin-fixed paraffin-embedded (FFPE) tissue sections were stored and classified by the Pathology Division of the Arcispedale S. Maria Nuova IRCCS, Reggio Emilia, Italy. IHC was performed on 4 µm-thick formalin-fixed, paraffin-embedded sections of 3 ALK^- ALCL using anti-SOD1 (#37385, Rabbit Monoclonal, Cell Signaling Technology, 1:800) monoclonal primary antibody. The immunohistochemical staining was developed on platform Ventana Bench-ULTRA using the OptiView DAB Detection Kit (Ventana-Roche,Tucson, Az) and

amplified with OptiView Amplification Kit (Ventana-Roche,Tucson Az). Slides were counterstained with Hematoxylin II counterstain and Bluing Reagent. The IHC have been evaluated independently by two Pathologists (M.Z and S.A.). ALK$^-$ ALCL FFPE sections were considered SOD1-positive when at least 50% of the cells expressed this antigen. Diagnoses were assigned according to the WHO classification[1].

Supplementary Figure Legends

Supplementary Figure 1. Coding and non-coding profiling of ALCLs

(**A**) Boxplots representing the expression of ALK, BATF3, TMOD1, TNFRSF8 among ALK$^+$ (red) and ALK$^-$ (grey) ALCL evaluated by nCounter platform in the FFPE cohort. Comparisons were considered significant for p≤0.05 (*). (**B**) Boxplot representing the expression of ERBB4 among ALK$^+$ (red) and ALK$^-$ (grey) ALCL evaluated by nCounter platform in the FFPE cohort. Comparison was considered significant for p≤0.05 (*). (**C**) Dot plots show gene expression counts distribution of the six not statistically significant lncRNAs among ALK$^+$ ALCL (red dots) and ALK$^-$ ALCL (black dots) of the FFPE training cohort. (**D**) Graphs show the expression of lncRNAs among ALK$^+$ (red) and ALK$^-$ (grey) ALCL evaluated by RT-qPCR in the validation cohort. (**E**) RT-qPCR analysis expression of MTAAT level in donor resting (n=3) and activated (n=3) CD4+ T-lymphocytes. (**F**) Graph shows the high discriminatory accuracy (70%) of the ROC curve.

Supplementary Figure 2. Regulatory features of MTAAT

(A) RT-qPCR analysis expression of MTAAT level in a panel of cell lines. (**B**) ChIP-PCR detection of IgG on MTAAT fragments in ALK$^-$ ALCL cell lines. GAPDH promoter was used as CTR+ whereas a non-coding intergenic region (CTR−) served as negative control. The values are representative of three independent experiments. (**C**) ChIP-PCR detection of RNAPII, H3K4me3, and H3K27Ac markers on MTAAT fragments in MTAAT-negative cell line

CUTLL1. GAPDH promoter was used as CTR+ whereas a noncoding intergenic region (CTR−) served as negative control. The values are representative of three independent experiments.

Supplementary Figure 3. Functional validation of MTAAT KD through CRISPR dCAS9-KRAB system

(**A**) Relative expression of OIPS5-AS1, DANCR, NEAT1, and KCNQ1OT1 used as controls for cytoplasmic, nucleic, and chromatinic fractions, respectively (representative three independent experiment). **(B)** Dot plots show physical parameters and setting strategy to sort ALCL dCas9-KRAB cells expressing MTAAT-sgRNA-GFP guides. **(C)** Western blot shows time course expression of dCAS9-KRAB-HA after doxycycline treatment. (**D**) RT-qPCR analysis of MTAAT expression 48 hours after doxycycline treatment in TLBR-2 dCAS9-KRAB ($MTAAT^{KD}$) and MAC2A dCAS9-KRAB ($MTAAT^{KD}$). Comparison was considered significant for $p \leq 0.01$ (**). (**E**) RT-qPCR expression analysis of a panel of MTAAT-target genes in ALCL dCas9-KRAB cells expressing sgRNA#3 (48 hours after doxycycline treatment). Comparison was considered significant for $p \leq 0.05$ (*) and $p \leq 0.01$ (**).

Supplementary Figure 4. Loss of MTAAT promotes RNAPII recruitment on its target genes.

(**A**) Graphs show the TSS and fragments around TSS of a set of genes deregulated after $MTAAT^{KD}$ ChIP-qPCR detection of H3K4me3 (**B**), H3K27Ac (**C**) and RNAPII (**D**) on MTAAT-genes target fragments in TLBR-2 $MTAAT^{KD}$ cell lines. The values are representative of three independent experiments. (**E**) RT-qPCR analysis of OPTN expression after MTAAT-KD (48 hours after doxycycline treatment) in TLBR-2 dCAS9-KRAB cells. (**F**) Graph shows interaction propensities of MTAAT with a set of chromatin modifier enzyme. In red, a representative group of H3K4-modifier proteins and in blue, a representative group of H3K9-

modifier proteins. In green, the most important catalytic subunit of RNAPII. The interaction propensity between EZH2 and HOTTIP was used as CTR+ whereases the interaction propensity between Wdr5 and HYMAI was set as CTR-. (**G**) RT-qPCR expression analysis of MTAAT and BNIP3 expression in a panel of non-TCL cell lines (thyroid cancer, purple; lung cancer, blue; breast, red; diffuse large B cell lymphoma, green).

Supplementary Figure 5. Loss of MTAAT does not affect cell cycle nor apoptosis

(**A**) Representative immunohistochemistry analysis of SOD1 in FFPE section of ALK^{-}ALCL patients expressing different level of MTAAT. Magnification 200X. (**B**) Western blots show the expression of autophagic markers after 48hr of MTAAT KD in TLBR-2 and MAC2A dCas9-KRAB sgRNA#3 cells. Densitometric analysis of LC3 refers to LC3II band. Cloroquine (CQ) was added to cells for the last for 2 hours of doxycycline -DOX- treatment (20μM for TLBR-2 and 40μM for MAC2A). (**C**) Histograms show the percentage of cell in each cell cycle phase (72 hours after doxycycline -DOX- treatment). (**D**) Western blot shows the expression of CASP3 and PARP-1 in TLBR-2 MTAAT^{KD} (72 hours after doxycycline treatment).

Supplementary Table

Supplementary Table 1. List of primers used in this study

Primer qPCR MTAAT Promoter	
KpnI_MTAAT Prom F	atcaaggtaccggtaccGTGTCTCCTCAACAGC TGTG
XhoI_MTAAT Prom R	gttcactcgagctcgagACAACGTGCCAGAATCT GTG

Primer lncRNAs	**Sequence (5'-3')**
XLOC_115902 F	TGGGTCACCAGTTCTGCTCT
XLOC_115902 R	AAGGGTGCTGTTTTGAGTGC
XLOC_066584 F	AGGAACTCTACTCAAGATTCTGGG
XLOC_066584 R	TCACTGTAAGTTAGATCAACGGGT
XLOC_211989 F	ATTTGACCCCTCTGCACCTG
XLOC_211989 R	TGCCAGGATGTATGGGTTCTG
XLOC_215396 F	GGATGCACTTGTCAGGGTAGG
XLOC_215396 R	GGTACTTGTCCCTACACCCCC
XLOC_261766 F	ACATACCTTTCCGTAGAGCAGT
XLOC_261766 R	CAAAGGTCTCAAAGCGGTCC
XLOC_136653 F	ATGCCAAACTGTACCCTGCC
XLOC_136653 R	TGCTTTTGTGTCCAAGGGGT
DANCR F	GAAGTGCAGCTGCCTCAGTTCTTA
DANCR R	AATGGCTTGTGCCTGTAGTTGTC
NEAT1 F	CTTCTTCCCTTTAACTTATCCATTCAC
NEAT1 R	CTCTTCCTCCACCATTACCAACAATAC
KCNQ1OT1 F	GGCTACGACCACAGGTGAAA
KCNQ1OT1 R	GTCTGCTGGCTTGTGTGTTG
OIP5-AS1 F	TTTCCTTGACCTTTAGGTGCTTT
OIP5-AS1 R	GAAGCAGGACTACCCACTCTAGG

Primers RNAseq validation	**Sequence (5'-3')**
BNIP3 F	CGGGATGCAGGAGGAGAG
BNIP3 R	TAGAAACCGAGGCTGGAACG

BNIP3L F	CAGCAGGGACCATAGCTCTC
BNIP3L R	TGATACCCAGTCCGCACTTT
MAP1LC3B F	TTCAGGTTCACAAAACCCGC
MAP1LC3B R	TCTCACACAGCCCGTTTACC
GABARAP F	CGAAAGAAATACCCGGACCG
GABARAP R	GAGATCAGAAGGCACCAGGT
XBP1 F	CTGGAGCTATGGTGGTGGTG
XBP1 R	CCCCGACAGAAGCAGAACTT
TRIB3 F	CAGCGGATGCAGAGGAGAGA
TRIB3 R	GCCGTCTGATGCCCTCG
ATF4 F	GAAGCGATTTAACGAGCGCC
ATF4 R	ATCTTGGTTCCTGCCACGTT
ALDOC F	GGGCGCTTACCTTCTCCTAT
ALDOC R	ACTGCCTTCATACTTGCCCT
PGM1 F	TGGGAAAGCAGCAGTTTGAC
PGM1 R	CCCACAACTCCATGCATAGC
PFKB3 F	CACTTGCATTACCGTCCCTG
PFKB3 R	ACTCTTCCGACCTTCCCAAG
TPI1 F	GGGGCTTTTACTGGGGAGAT
TPI1 R	CCAATGCAGGCGATTACTCC
GPI F	AAGACAATAGTGGGGTGGGG
GPI R	TTGTCCAGGAATTCACCCGA
MPI F	AGGAAAGGGAAAGGGTAGGC
MPI R	TGTAGGGAGGGCTCTTTTGG
OPTN F	TTGGAGTGACTTTTCCACAGGA

OPTN R	GGGGCTGTCCTCCTTTTCAG
CHMP2A F	ATGGACCTATTGTTCGGGCG
CHMP2A R	TCTCTAGTTTCTGTCGCTCGC

Primer ChIP	**Sequence (5'-3')**
P6 MTAAT F	TACTGGGGGAAACAGCAAAC
P6 MTAAT R	TGTGGGACACAGCTAAAGCA
P3 MTAAT F	GCCTCTGCCATGCCCTAATA
P3 MTAAT R	GATTCTTTATCTGCTGTCTGTGC
P4 MTAAT F	TCTCACCATTGTTCAAACTGCT
P4 MTAAT R	GGGTCTTGAGCTATGTGACG
P5 MTAAT F	TCCTCTGAATGATCTCTGTCTGT
P5 MTAAT R	TTGCTGCTCTGACTGTTCCA
P1 BNIP3 F	CTCTCCTCCTGCATCCCG
P1 BNIP3 R	CTGCCCTGTGAGTTCCTCC
P2 BNIP3 F	TGCTAGTGGGGAAACTGAGG
P2 BNIP3 R	TCCCGAGACGCTCAGCTC
P3 BNIP3 F	TCCCGAGACGCTCAGCTC
P3 BNIP3 R	GACCCCGGTTCAGCTTCT
P4 BNIP3 F	ACCGCCAGAGATACATAGCA
P4 BNIP3 R	GGAGTCTTTCTGTGTTGCCA
P1 BNIP3L F	TCCCCAAGACACCTATTGCA
P1 BNIP3L R	GCAGTGGGAGAGAGGATGAG
P2 BNIP3L F	GCGAGGAAAATGAGCAGTCT
P2 BNIP3L R	GCCAATGAGCTGCCTTCTC

P3 BNIP3L F	TCGTCTAGGGTTGGCTTCAG
P3 BNIP3L R	ATCTTGGGTGGTTCAGGAGG
P1 ATF4 F	GCACTTGAGCCGGATGAAAA
P1 ATF4 R	TTTCCAGAGGCCCCATTCAT
P2 ATF4 F	CAGGCCACAAATCACCACC
P2 ATF4 R	GGTCGCTGCTAGTCCTCAG
P3 ATF4 F	CGTCCTCGGCCTTCACAATA
P3 ATF4 R	TCACGAAAGGAGAGAGGTGT
P1 XBP1 F	CCAAACCGAGAGCTTTCCAG
P1 XBP1 R	GTCTTTTCGAACCCAAGGCC
P2 XBP1 F	GTTTCAGGACCGTGGCTATG
P2 XBP1 R	TCAGTCTGGAAAGCTCTCGG
P1 OPTN F	GCCTGGCATTCTCCTCTTTC
P1 OPTN R	GCTCTAAGGCGTCACTGTGA
P2 OPTN F	ATGGGCGGGGTATGGGAT
P2 OPTN R	GTCACTGTTTCCTCGGCATC
P3 OPTN F	GCGGCCTGAAAACGGTAC
P3 OPTN R	ACGTCACCTCCAAGTCTCTG
GAPDH Exon1 F	AAGACCTTGGGCTGGGACT
GAPDH Exon1 R	GCTGCGGGCTCAATTTATAG
RUNX2 Upstream F	TCTCAAGGTGCCTGTCTGC
RUNX2 Upstream R	TGAAGTTTGGCCTCTGGTCT
D17Z1 (α-Sat) F	CTTTGGATGGAGCAGGTTTGAGAC
D17Z1 (α-Sat) R	CCGTTTAGTTAGGTGCAGTTATCC

Supplementary Table 2. List of sgRNA and GapmeRs sequences

sg_RNA	Primer Forward	Primer Reverse
sgRNA_MTAAT #2	CACCGTAATCTTCTGAGGTTGCTGA	AAACTCAGCAACCTCAGAAGATTAC
sgRNA_MTAAT #3	CACCGGCACCTACTGTGTATTTCCT	AAACTCAGCAACCTCAGAAGATTAC

GapmeR	Sequence	Cat.no. * Qiagen
Negative control	AACACGTCTATACGC	339515
lncRNA_MTAAT #1	TCATTAGCTAGGAGTA	339511
lncRNA_MTAAT #2	TCAATAAAGCGGGATC	339511

Supplementary Table 3. List of genes analysed by nCounter platform

Gene	Type
XLOC_043524	lncRNA
XLOC_066584	lncRNA
XLOC_080485	lncRNA
XLOC_098415	lncRNA
XLOC_115902	lncRNA
XLOC_163319	lncRNA

XLOC_169868	lncRNA
XLOC_136653	lncRNA
XLOC_169876	lncRNA
XLOC_177839	lncRNA
XLOC_211989	lncRNA
XLOC_215396	lncRNA
XLOC_261766	lncRNA
XLOC_286804	lncRNA
XLOC_330767	lncRNA
XLOC_330840	lncRNA
XLOC_334219	lncRNA
ERBB4	lncRNA
ALK	Coding gene
TMOD	Coding gene
BATF3	Coding gene
TNFRSF8	Coding gene
BNIP3	Coding gene
BNIP3L	Coding gene
CHMP2A	Coding gene/housekeeping
REEP5	Coding gene/housekeeping
EMC7	Coding gene/housekeeping

COG7	Coding gene/housekeeping
DNAJC14	Coding gene/housekeeping
EIF2B4	Coding gene/housekeeping
ERCC3	Coding gene/housekeeping
G6PD	Coding gene/housekeeping
GUSB	Coding gene/housekeeping
MRPS5	Coding gene/housekeeping
PPIA	Coding gene/housekeeping
MTMR14	Coding gene/housekeeping
HPRT1	Coding gene/housekeeping
SF3A3	Coding gene/housekeeping
TLK2	Coding gene/housekeeping

Supplementary Table 4. Expression level of genes used to classify ALCL patients

Sample	ALK traslocation	BATF3	TMOD1	TNFRSF8	Other translocation	ALCL Classification
lt2	+	-	-	-	-	ALK+
lt3	+	+	-	+	-	ALK+
lt4	+	+	+	+	-	ALK-
lt5	+	+	+	+	-	ALK-
lt6	-	+	+	+	-	ALK-
lt7	+	+	+	+	-	ALK+
lt8	-	+	-	+	-	ALK-
lt9	+	+	+	+	-	ALK+
lt10	-	-	-	-	-	ALK-
lt11	+	+	+	+	-	ALK-
lt12	+	+	+	+	-	ALK-
lt13	+	-	-	-	-	ALK+
lt14	-	+	-	+	-	ALK-
lt15	+	+	+	+	-	ALK-
lt17	-	+	+	-	-	ALK-
lt19	+	+	+	+	-	ALK+
lt20	-	-	-	-	-	ALK-
lt21	+	+	+	+	-	ALK+
lt22	+	+	+	+	-	ALK-
lt23	+	+	+	+	-	ALK+
lt24	-	-	-	-	+	ALK+
lt25	+	+	-	+	-	ALK+
lt26	+	+	+	+	-	ALK+
lt27	+	+	+	+	-	ALK-
lt28	+	+	+	+	-	ALK+
lt29	-	-	-	-	-	ALK-
lt30	-	-	+	+	-	ALK-
lt31	+	+	+	+	-	ALK-
lt32	+	+	+	+	-	ALK-
lt34	+	+	+	+	-	ALK-
lt35	+	+	+	+	-	ALK-
lt36	+	+	+	+	-	ALK-
lt37	+	+	+	+	-	ALK-
lt38	+	+	+	+	-	ALK-
lt39	+	+	-	+	-	ALK+
lt40	+	-	-	+	-	ALK+
lt42	-	-	+	+	-	ALK-
lt44	+	+	+	+	-	ALK-
lt45	-	-	+	-	-	ALK-
lt47	+	+	+	+	-	ALK+
lt48	+	+	+	+	-	ALK-
lt50	+	+	+	+	-	ALK-
lt51	+	+	+	+	-	ALK-
lt52	-	-	+	-	-	ALK-

Supplementary Table 5. In silico analysis of MTAAT open reading frames (ORFs)

Label	Strand	Frame	Start	Stop	Lenght (nt|aa)
ORF1	+	1	4012	4182	171|56
ORF2	+	3	2127	2285	159|52
ORF3	-	1	5266	5072	195|64
ORF4	-	1	2620	2429	192|63

Supplementary Table 6. TF binding sites prediction by FIMO algorithm

motif	sequence	start	stop	score	p.value	q.value	matched_sequence	database
IRF3	chr3:180332773-180333239	347	366	18,5372	2,04E-07	0,000171	GAAGAGGAAAGGAAAAGGGT	HOCOMOCO
ZKSC1	chr3:180332773-180333239	270	288	17,3438	6,69E-07	0,000589	TAAGCACCTACTGTGTATT	HOCOMOCO
ZFP82	chr3:180332773-180333239	347	370	16,3833	0,00000119	0,000984	TTCCACCCTTTTCCTTTCCTCTTC	HOCOMOCO
IRF3	chr3:180332773-	346	365	16,0744	0,00000155	0,000648	AGAAGAGGAAAGGAAAAGGG	HOCOMOCO

	180333239							
ZN467	chr3:18033 2773-180333239	347	368	13,734	0,000 00235	0,00 15	GAAGAGGAAAGG AAAAGGGTGG	HOCO MOCO
MAZ	chr3:18033 2773-180333239	361	382	14,55 08	0,000 00282	0,00 236	AAGGGTGGAACA GTCAGAGCAG	HOCO MOCO
NR1H3	chr3:18033 2773-180333239	165	183	14,84 56	0,000 00313	0,00 275	CTGAGGTTGCTGA AGGCCC	HOCO MOCO
FLI1	chr3:18033 2773-180333239	350	367	15,17 19	0,000 00316	0,00 267	GAGGAAAGGAAA AGGGTG	HOCO MOCO
ZN467	chr3:18033 2773-180333239	350	371	12,88 3	0,000 00358	0,00 15	GAGGAAAGGAAA AGGGTGGAAC	HOCO MOCO
ETS2	chr3:18033 2773-180333239	353	365	13,95 31	0,000 00376	0,00 324	GAAAGGAAAAGG G	HOCO MOCO
ETV5	chr3:18033 2773-180333239	352	365	14,04 76	0,000 00569	0,00 264	GGAAAGGAAAAG GG	HOCO MOCO
ZN394	chr3:18033 2773-180333239	352	371	13,36 62	0,000 00604	0,00 43	GGAAAGGAAAAG GGTGGAAC	HOCO MOCO

ETV5	chr3:18033 2773-180333239	347	360	13,95 24	0,000 0062	0,00 264	GAAGAGGAAAGG AA	HOCO MOCO
BC11A	chr3:18033 2773-180333239	346	362	13,89 17	0,000 00624	0,00 526	AGAAGAGGAAAG GAAAA	HOCO MOCO
CRX	chr3:18033 2773-180333239	226	238	13,87 5	0,000 00633	0,00 55	TCAGAGGATTAAG	HOCO MOCO
IRF1	chr3:18033 2773-180333239	70	89	14,09 38	0,000 00675	0,00 585	AAAAATGAAAATG AAAATGT	HOCO MOCO
OTX2	chr3:18033 2773-180333239	226	236	13,69 47	0,000 00678	0,00 593	AGAGGATTAAG	HOCO MOCO
KLF3	chr3:18033 2773-180333239	357	375	12,92 19	0,000 00718	0,00 615	GGAAAAGGGTGG AACAGTC	HOCO MOCO
ANDR	chr3:18033 2773-180333239	46	63	13,85 12	0,000 00723	0,00 631	AGTTCTGTCAAGT TTGCT	HOCO MOCO
ZFX	chr3:18033 2773-180333239	163	172	14,32 81	0,000 00851	0,00 771	GAAGGCCCCA	HOCO MOCO
ZN341	chr3:18033	353	374	13,07	0,000	0,00	GAAAGGAAAAGG	HOCO

	2773-180333239			69	00881	348	GTGGAACAGT	MOCO
ZN341	chr3:18033 2773-180333239	362	383	13,05 13	0,000 00894	0,00 348	AGGGTGGAACAG TCAGAGCAGC	HOCO MOCO
VEZF1	chr3:18033 2773-180333239	348	369	13,01 48	0,000 00902	0,00 482	AAGAGGAAAGGA AAAGGGTGGA	HOCO MOCO
CDX2	chr3:18033 2773-180333239	379	390	13,06 67	0,000 0091	0,00 828	CTTTATTGCTGC	HOCO MOCO
ZN394	chr3:18033 2773-180333239	347	366	12,81 69	0,000 0103	0,00 43	GAAGAGGAAAGG AAAAGGGT	HOCO MOCO
KLF15	chr3:18033 2773-180333239	350	368	11,25	0,000 0104	0,00 904	GAGGAAAGGAAA AGGGTGG	HOCO MOCO
SP4	chr3:18033 2773-180333239	356	375	12,75 21	0,000 0107	0,00 915	AGGAAAAGGGTG GAACAGTC	HOCO MOCO
MAZ	chr3:18033 2773-180333239	346	367	12,04 24	0,000 0115	0,00 479	AGAAGAGGAAAG GAAAAGGGTG	HOCO MOCO
VEZF1	chr3:18033 2773-	344	365	12,59 26	0,000 0116	0,00 482	GCAGAAGAGGAA AGGAAAAGGG	HOCO MOCO

	180333239							
ZN467	chr3:18033 2773-180333239	344	365	10,39 36	0,000 0117	0,00 324	GCAGAAGAGGAA AGGAAAAGGG	HOCO MOCO
ZN350	chr3:18033 2773-180333239	350	367	12,93 94	0,000 012	0,01 01	CACCCTTTTCCTT TCCTC	HOCO MOCO
IRF9	chr3:18033 2773-180333239	410	421	13,47 11	0,000 0121	0,01 1	AAAAGAGAAATT	HOCO MOCO
ZN341	chr3:18033 2773-180333239	343	364	12,46 15	0,000 0126	0,00 348	TGCAGAAGAGGA AAGGAAAAGG	HOCO MOCO
LYL1	chr3:18033 2773-180333239	158	171	12,46 15	0,000 0146	0,01 27	CCTTCTGGGGCC TT	HOCO MOCO
LEF1	chr3:18033 2773-180333239	346	359	12,15 15	0,000 0168	0,01 46	TCCTTTCCTCTTC T	HOCO MOCO
SPI1	chr3:18033 2773-180333239	345	361	12,42 19	0,000 0169	0,01 44	CAGAAGAGGAAA GGAAA	HOCO MOCO
VEZF1	chr3:18033 2773-180333239	343	364	11,71 11	0,000 0195	0,00 538	TGCAGAAGAGGA AAGGAAAAGG	HOCO MOCO

ZN257	chr3:180332773-180333239	349	360	12,5156	0,0000208	0,0182	TTCCTTTCCTCT	HOCOMOCO
IRF2	chr3:180332773-180333239	70	89	11,3906	0,0000209	0,0181	AAAAATGAAAATGAAAATGT	HOCOMOCO
FLI1	chr3:180332773-180333239	345	362	11,8906	0,0000214	0,00903	CAGAAGAGGAAAGGAAAA	HOCOMOCO
FOXJ3	chr3:180332773-180333239	103	115	13,0469	0,0000214	0,0188	ATGTTTTTGTTTG	HOCOMOCO
BC11A	chr3:180332773-180333239	423	439	12,2667	0,0000234	0,00988	GATACAGGAACTCAGAA	HOCOMOCO
STAT6	chr3:180332773-180333239	261	271	12,5619	0,0000235	0,0206	TGCCCAGGAAA	HOCOMOCO
PRDM1	chr3:180332773-180333239	353	366	12,4375	0,0000239	0,0207	GAAAGGAAAAGGGT	HOCOMOCO
ERG	chr3:180332773-180333239	347	359	12,5781	0,0000239	0,0169	GAAGAGGAAAGGA	HOCOMOCO
PATZ1	chr3:18033	350	371	10,84	0,000	0,02	GAGGAAAGGAAA	HOCO

	2773-180333239			03	0256	16	AGGGTGGAAC	MOCO
ZN140	chr3:18033 2773-180333239	360	383	9	0,000 0262	0,02 27	GCTGCTCTGACTG TTCCACCCTTT	HOCO MOCO
MAZ	chr3:18033 2773-180333239	349	370	10,41 53	0,000 0269	0,00 748	AGAGGAAAGGAA AAGGGTGGAA	HOCO MOCO
SPIB	chr3:18033 2773-180333239	345	361	10,62 5	0,000 0273	0,01 49	CAGAAGAGGAAA GGAAA	HOCO MOCO
ETV4	chr3:18033 2773-180333239	348	358	12,39 06	0,000 0274	0,02 39	AAGAGGAAAGG	HOCO MOCO
ETV2	chr3:18033 2773-180333239	350	365	11,54 41	0,000 028	0,02 44	GAGGAAAGGAAA AGGG	HOCO MOCO
IRF4	chr3:18033 2773-180333239	422	439	11,35 79	0,000 0294	0,01 36	GATACAGGAACTC AGAAT	HOCO MOCO
ZN341	chr3:18033 2773-180333239	344	365	10,82 91	0,000 0312	0,00 647	GCAGAAGAGGAA AGGAAAAGGG	HOCO MOCO
BATF3	chr3:18033 2773-	415	431	12,04 62	0,000 0312	0,02 77	CTCTTTTATTCTG AGTT	HOCO MOCO

	180333239							
ZIC3	chr3:18033 2773-180333239	273	287	11,02 74	0,000 0314	0,02 8	AAGCACCTACTGT GT	HOCO MOCO
IRF4	chr3:18033 2773-180333239	346	363	11,18 95	0,000 032	0,01 36	AGAAGAGGAAAG GAAAAG	HOCO MOCO
COE1	chr3:18033 2773-180333239	155	169	11,04 69	0,000 0336	0,02 94	AATCCTTCTGGGG CC	HOCO MOCO
KLF6	chr3:18033 2773-180333239	359	377	10,92 19	0,000 0337	0,02 95	AAAAGGGTGGAA CAGTCAG	HOCO MOCO
SPIB	chr3:18033 2773-180333239	424	440	10,03 12	0,000 0348	0,01 49	TGATACAGGAACT CAGA	HOCO MOCO
STAT2	chr3:18033 2773-180333239	68	86	11,17 19	0,000 0366	0,02 53	TTAAAAATGAAAA TGAAAA	HOCO MOCO
STF1	chr3:18033 2773-180333239	165	175	11,75 24	0,000 0372	0,03 33	GCTGAAGGCCC	HOCO MOCO
ZBT17	chr3:18033 2773-180333239	355	373	10,93 4	0,000 0384	0,01 14	AAGGAAAAGGGT GGAACAG	HOCO MOCO

ZBT17	chr3:180332773-180333239	350	368	10,8774	0,0000396	0,0114	GAGGAAAGGAAAAGGGTGG	HOCOMOCO
ERG	chr3:180332773-180333239	352	364	11,7031	0,000004	0,0169	GGAAAGGAAAAGG	HOCOMOCO
ETS1	chr3:180332773-180333239	352	364	11,5625	0,0000405	0,0351	GGAAAGGAAAAGG	HOCOMOCO
ZBT17	chr3:180332773-180333239	344	362	10,8302	0,0000407	0,0114	GCAGAAGAGGAAAGGAAAA	HOCOMOCO
MAZ	chr3:180332773-180333239	344	365	9,50847	0,0000423	0,00884	GCAGAAGAGGAAAGGAAAAGGG	HOCOMOCO
ZN502	chr3:180332773-180333239	353	372	2,90411	0,0000425	0,0373	GAAAGGAAAAGGGTGGAACA	HOCOMOCO
NR4A2	chr3:180332773-180333239	114	122	11,9195	0,0000432	0,0394	AAAGGTCAT	HOCOMOCO
SMCA5	chr3:180332773-180333239	38	52	11,339	0,0000433	0,0379	GAAGAGAGAGCAAAC	HOCOMOCO
NR4A1	chr3:18033	114	122	11,15	0,000	0,03	AAAGGTCAT	HOCO

	2773-180333239			33	0448	92		MOCO
HXC9	chr3:180332773-180333239	381	390	11,6355	0,0000458	0,0416	CTTTATTGCT	HOCOMOCO
ZN467	chr3:180332773-180333239	351	372	7,24468	0,0000461	0,00914	AGGAAAGGAAAAGGGTGGAACA	HOCOMOCO
BATF	chr3:180332773-180333239	97	114	11,5231	0,0000462	0,0411	TGTTTTTGTTTGACTAAT	HOCOMOCO
VEZF1	chr3:180332773-180333239	349	370	10,1704	0,0000462	0,00789	AGAGGAAAGGAAAAGGGTGGAA	HOCOMOCO
RXRG	chr3:180332773-180333239	114	126	8,79688	0,0000469	0,0419	CTTAAAAGGTCAT	HOCOMOCO
VEZF1	chr3:180332773-180333239	358	379	10,1185	0,0000475	0,00789	GAAAAGGGTGGAACAGTCAGAG	HOCOMOCO
ZN350	chr3:180332773-180333239	388	405	11,2626	0,0000481	0,0203	GAGTTCATTTCTTACCTT	HOCOMOCO
LEF1	chr3:180332773-	351	364	11,1212	0,0000498	0,0217	CCTTTTCCTTTCCT	HOCOMOCO

	180333239							
ZN143	chr3:18033 2773-180333239	139	160	7,151 16	0,000 05	0,04 45	AGGATTTGGGTAG ATGTATTTC	HOCO MOCO
PRDM6	chr3:18033 2773-180333239	353	365	11,54 69	0,000 0513	0,04 13	GAAAGGAAAAGG G	HOCO MOCO
ZN274	chr3:18033 2773-180333239	32	51	9,865 55	0,000 0515	0,02 89	GCCACTGAAGAG AGAGCAAA	HOCO MOCO
IRF1	chr3:18033 2773-180333239	408	427	10,21 88	0,000 0522	0,01 54	CAGAATAAAAGAG AAATTAT	HOCO MOCO
IRF1	chr3:18033 2773-180333239	347	366	10,17 19	0,000 0534	0,01 54	GAAGAGGAAAGG AAAAGGGT	HOCO MOCO
SPI1	chr3:18033 2773-180333239	424	440	9,953 12	0,000 0545	0,02 32	TGATACAGGAACT CAGA	HOCO MOCO
ZN467	chr3:18033 2773-180333239	362	383	6,829 79	0,000 0548	0,00 914	AGGGTGGAACAG TCAGAGCAGC	HOCO MOCO
BC11A	chr3:18033 2773-180333239	351	367	11,10 83	0,000 0553	0,01 55	AGGAAAGGAAAA GGGTG	HOCO MOCO

NR6A1	chr3:180332773-180333239	109	121	9,37209	0,0000562	0,0499	AAGGTCATGTTTT	HOCOMOCO
NR1I2	chr3:180332773-180333239	398	416	10,6977	0,0000588	0,052	AGAAATTATAAGAGTTCAT	HOCOMOCO
IRF3	chr3:180332773-180333239	70	89	10,562	0,0000589	0,0165	AAAAATGAAAATGAAAATGT	HOCOMOCO
RFX1	chr3:180332773-180333239	163	184	7,57812	0,0000592	0,0511	TCTGAGGTTGCTGAAGGCCCCA	HOCOMOCO
STAT2	chr3:180332773-180333239	350	368	10,2031	0,0000592	0,0253	GAGGAAAGGAAAAGGGTGG	HOCOMOCO
ELF5	chr3:180332773-180333239	345	359	10,8906	0,0000597	0,0515	CAGAAGAGGAAAGGA	HOCOMOCO
PATZ1	chr3:180332773-180333239	362	383	9,13445	0,0000623	0,0263	AGGGTGGAACAGTCAGAGCAGC	HOCOMOCO
ZN816	chr3:180332773-180333239	359	379	8,07812	0,0000628	0,0324	AAAAGGGTGGAACAGTCAGAG	HOCOMOCO
ZN121	chr3:18033	162	181	5,095	0,000	0,05	CTGGGGCCTTCA	HOCO

	2773-180333239			24	0632	53	GCAACCTC	MOCO
ZN263	chr3:180332773-180333239	366	385	8,4375	0,0000657	0,0566	TGGAACAGTCAGAGCAGCAA	HOCOMOCO
ZN335	chr3:180332773-180333239	354	375	8,67568	0,0000657	0,056	GACTGTTCCACCCTTTTCCTTT	HOCOMOCO
ZN490	chr3:180332773-180333239	332	355	-8,625	0,0000665	0,0571	TTCCTCTTCTGCAGGCAAAAGATA	HOCOMOCO
ZN274	chr3:180332773-180333239	341	360	9,36975	0,0000665	0,0289	CCTGCAGAAGAGGAAAGGAA	HOCOMOCO
NFAC1	chr3:180332773-180333239	350	364	11,0762	0,0000689	0,0591	GAGGAAAGGAAAAGG	HOCOMOCO
ZN341	chr3:180332773-180333239	359	380	9,26496	0,0000706	0,0117	AAAAGGGTGGAACAGTCAGAGC	HOCOMOCO
ETS2	chr3:180332773-180333239	348	360	10,9844	0,0000708	0,0305	AAGAGGAAAGGAA	HOCOMOCO
ETV4	chr3:180332773-	263	273	11,1562	0,0000715	0,0312	CCCAGGAAATA	HOCOMOCO

	180333239							
NR2C1	chr3:18033 2773-180333239	114	126	10,04 26	0,000 0721	0,06 33	CTTAAAAGGTCAT	HOCO MOCO
IRF2	chr3:18033 2773-180333239	408	427	8,515 62	0,000 0735	0,02 7	CAGAATAAAAGAG AAATTAT	HOCO MOCO
PAX6	chr3:18033 2773-180333239	1	12	10,85 95	0,000 0738	0,06 6	TCTCACTTGAGT	HOCO MOCO
COT2	chr3:18033 2773-180333239	111	123	10,84 38	0,000 0749	0,06 67	AAAAGGTCATGTT	HOCO MOCO
AP2A	chr3:18033 2773-180333239	164	178	9,656 25	0,000 0753	0,06 64	GGGGCCTTCAGC AAC	HOCO MOCO
ZN816	chr3:18033 2773-180333239	358	378	7,625	0,000 0758	0,03 24	GAAAAGGGTGGA ACAGTCAGA	HOCO MOCO
KLF15	chr3:18033 2773-180333239	362	380	6,609 38	0,000 0761	0,02 22	AGGGTGGAACAG TCAGAGC	HOCO MOCO
KLF15	chr3:18033 2773-180333239	351	369	6,593 75	0,000 0766	0,02 22	AGGAAAGGAAAA GGGTGGA	HOCO MOCO

GCR	chr3:18033 2773-180333239	367	381	10,4688	0,0000779	0,0679	TGCTCTGACTGTTCC	HOCOMOCO
ZN214	chr3:18033 2773-180333239	221	242	10,36	0,0000783	0,0687	CAGATCTTAATCCTCTGAATGA	HOCOMOCO
SMAD3	chr3:18033 2773-180333239	36	47	10,678	0,0000806	0,0718	CTCTCTCTTCAG	HOCOMOCO
PTF1A	chr3:18033 2773-180333239	158	175	9,70476	0,0000812	0,0701	CCTTCTGGGGCCTTCAGC	HOCOMOCO
PRDM1	chr3:18033 2773-180333239	347	360	10,2344	0,0000815	0,028	GAAGAGGAAAGGAA	HOCOMOCO
IRF7	chr3:18033 2773-180333239	353	362	10,9111	0,000082	0,0398	GAAAGGAAAA	HOCOMOCO
ETV2	chr3:18033 2773-180333239	260	275	8,98529	0,0000826	0,036	GTGCCCAGGAAATACA	HOCOMOCO
IRF3	chr3:18033 2773-180333239	414	433	9,90083	0,0000854	0,0179	GGAACTCAGAATAAAAGAGA	HOCOMOCO
ZNF76	chr3:18033	154	175	7,282	0,000	0,07	AAATCCTTCTGGG	HOCO

	2773-180333239			05	0859	58	GCCTTCAGC	MOCO
BCL6	chr3:18033 2773-180333239	197	209	10,4769	0,0000864	0,0772	TGTTGTCTAGGGA	HOCO MOCO
HSF1	chr3:18033 2773-180333239	160	174	9,75	0,0000873	0,0772	CTGAAGGCCCCA GAA	HOCO MOCO
NR5A2	chr3:18033 2773-180333239	165	175	10,1406	0,0000876	0,0787	GCTGAAGGCCC	HOCO MOCO
IRF7	chr3:18033 2773-180333239	76	85	10,8444	0,0000883	0,0398	GAAAATGAAA	HOCO MOCO
STAT2	chr3:18033 2773-180333239	74	92	9,29688	0,0000908	0,0259	ATGAAAATGAAAA TGTACT	HOCO MOCO
MAZ	chr3:18033 2773-180333239	350	371	7,92373	0,0000909	0,0152	GAGGAAAGGAAA AGGGTGGAAC	HOCO MOCO
KLF5	chr3:18033 2773-180333239	362	375	8,95312	0,000092	0,0822	AGGGTGGAACAG TC	HOCO MOCO
ZN467	chr3:18033 2773-	352	373	5,54255	0,0000923	0,0128	GGAAAGGAAAAG GGTGGAACAG	HOCO MOCO

	180333239							
PRDM6	chr3:18033 2773-180333239	348	360	10,875	0,0000929	0,0413	AAGAGGAAAGGAA	HOCOMOCO
IRF2	chr3:18033 2773-180333239	347	366	7,90625	0,000094	0,027	GAAGAGGAAAGGAAAAGGGT	HOCOMOCO
IRF8	chr3:18033 2773-180333239	420	439	8,60938	0,0000967	0,0421	GATACAGGAACTCAGAATAA	HOCOMOCO
PRDM1	chr3:18033 2773-180333239	352	365	9,89062	0,0000968	0,028	GGAAAGGAAAAGGG	HOCOMOCO
ELF3	chr3:18033 2773-180333239	346	359	10,0312	0,0000971	0,084	AGAAGAGGAAAGGA	HOCOMOCO
IRF8	chr3:18033 2773-180333239	70	89	8,5625	0,0000987	0,0421	AAAAATGAAAATGAAAATGT	HOCOMOCO
ZFP28	chr3:18033 2773-180333239	342	361	7,3125	0,0000994	0,0422	TTTCCTTTCCTCTTCTGCAG	HOCOMOCO
ZFP28	chr3:18033 2773-180333239	413	432	7,3125	0,0000994	0,0422	TTCTCTTTTATTCTGAGTTC	HOCOMOCO

ZNF263	chr3:18033 2773-180333239	349	369	13,5	0,000 0054	0,00 458	AGAGGAAAGGAA AAGGGTGGA	JASPA R
HIC2	chr3:18033 2773-180333239	260	268	13,67 92	0,000 00814	0,00 726	GTGCCCAGG	JASPA R
IRF1	chr3:18033 2773-180333239	71	91	13,7	0,000 00837	0,00 715	GTACATTTTCATTT TCATTTT	JASPA R
SP2	chr3:18033 2773-180333239	357	371	12,41 07	0,000 0108	0,00 916	GTTCCACCCTTTT CC	JASPA R
DMRT3	chr3:18033 2773-180333239	432	442	12,78 33	0,000 0116	0,01 03	CCTGTATCAAC	JASPA R
CRX	chr3:18033 2773-180333239	227	237	13,58 93	0,000 0136	0,01 2	CAGAGGATTAA	JASPA R
ZFX	chr3:18033 2773-180333239	158	171	12,23 44	0,000 0145	0,01 25	CCTTCTGGGGCC TT	JASPA R
IRF7	chr3:18033 2773-180333239	74	87	12,45	0,000 0148	0,01 31	ATGAAAATGAAAA T	JASPA R
ZNF263	chr3:18033	346	366	11,60	0,000	0,00	AGAAGAGGAAAG	JASPA

	2773-180333239			42	015	634	GAAAAGGGT	R
IRF3	chr3:18033 2773-180333239	345	365	7,547 95	0,000 0155	0,01 09	CAGAAGAGGAAA GGAAAAGGG	JASPA R
NR4A1	chr3:18033 2773-180333239	114	123	13,88 24	0,000 0165	0,01 5	AAAAGGTCAT	JASPA R
ZNF24	chr3:18033 2773-180333239	453	465	12,24 76	0,000 0167	0,01 48	AATTCATTTATTC	JASPA R
NR2F6(VAR.2)	chr3:18033 2773-180333239	115	129	- 0,205 882	0,000 0175	0,01 56	CTGCTTAAAAGGT CA	JASPA R
NR2F2	chr3:18033 2773-180333239	113	123	13,35 9	0,000 0196	0,01 77	AAAAGGTCATG	JASPA R
GSC2	chr3:18033 2773-180333239	226	235	11,60 34	0,000 0211	0,01 86	CTTAATCCTC	JASPA R
CDX2	chr3:18033 2773-180333239	380	390	13,17 74	0,000 0215	0,01 95	CAGCAATAAAG	JASPA R
GATA1: :TAL1	chr3:18033 2773-	330	347	12,69 81	0,000 0216	0,01 91	CATATCTTTTGCC TGCAG	JASPA R

	180333239							
IRF3	chr3:18033 2773-180333239	68	88	6,191 78	0,000 0249	0,01 09	TTAAAAATGAAAA TGAAAATG	JASPA R
BCL6	chr3:18033 2773-180333239	196	209	12,33 33	0,000 026	0,02 33	GTCCCTAGACAAC A	JASPA R
KLF5	chr3:18033 2773-180333239	362	371	11,18 75	0,000 0301	0,02 65	GTTCCACCCT	JASPA R
SP1	chr3:18033 2773-180333239	361	371	10,33 33	0,000 0332	0,02 92	GTTCCACCCTT	JASPA R
IRF1	chr3:18033 2773-180333239	348	368	10,85	0,000 0348	0,01 49	CCACCCTTTTCCT TTCCTCTT	JASPA R
IRF9	chr3:18033 2773-180333239	73	87	0,660 377	0,000 0359	0,03 17	AATGAAAATGAAA AT	JASPA R
ZNF263	chr3:18033 2773-180333239	350	370	9,645 83	0,000 0399	0,01 13	GAGGAAAGGAAA AGGGTGGAA	JASPA R
IRF8	chr3:18033 2773-180333239	74	87	- 0,056 6038	0,000 0435	0,03 92	ATGAAAATGAAAA T	JASPA R

GSC	chr3:180332773-180333239	226	235	11,5	0,0000475	0,0431	CTTAATCCTC	JASPAR
NR1H2::RXRA	chr3:180332773-180333239	113	129	-4,82979	0,0000506	0,044	CTGCTTAAAAGGTCATG	JASPAR
CDX1	chr3:180332773-180333239	382	390	10,8302	0,0000507	0,0464	GCAATAAAG	JASPAR
ZIC1	chr3:180332773-180333239	274	287	3,73913	0,0000532	0,0464	AAGCACCTACTGTG	JASPAR
FOXH1	chr3:180332773-180333239	267	277	11,5882	0,0000534	0,0474	GGAAATACACA	JASPAR
ELF1	chr3:180332773-180333239	262	273	8,22642	0,0000574	0,0513	GCCCAGGAAATA	JASPAR
ZNF263	chr3:180332773-180333239	376	396	8,66667	0,0000634	0,0134	AGAGCAGCAATAAAGGTAAGA	JASPAR
RORA	chr3:180332773-180333239	115	124	12,0319	0,0000663	0,0599	TAAAAGGTCA	JASPAR
ESRRA	chr3:18033	114	124	6,647	0,000	0,06	TAAAAGGTCAT	JASPA

	2773-180333239			06	0742	75		R
TCF7	chr3:18033 2773-180333239	347	358	9,333 33	0,000 0751	0,06 62	GAAGAGGAAAGG	JASPA R
MEIS2	chr3:18033 2773-180333239	53	60	11,12 5	0,000 0769	0,06 93	TTGACAGA	JASPA R
KLF1	chr3:18033 2773-180333239	362	372	8,859 38	0,000 0774	0,06 93	TGTTCCACCCT	JASPA R
IRF4	chr3:18033 2773-180333239	74	88	0,156 25	0,000 0776	0,06 99	ATGAAAATGAAAA TG	JASPA R
POU2F 2	chr3:18033 2773-180333239	72	84	10,69 64	0,000 0799	0,07	TTCATTTTCATTT	JASPA R
NR2F1	chr3:18033 2773-180333239	111	123	10,14 58	0,000 0806	0,07 31	AAAAGGTCATGTT	JASPA R
VDR	chr3:18033 2773-180333239	399	406	10,66 42	0,000 0815	0,07 46	AGAGTTCA	JASPA R
SMAD4	chr3:18033 2773-	199	206	12,13 33	0,000 0817	0,07 41	TGTCTAGG	JASPA R

	180333239							
IRF2	chr3:18033 2773-180333239	75	92	4,701 92	0,000 0818	0,07 29	TGAAAATGAAAAT GTACT	JASPA R
IRF1	chr3:18033 2773-180333239	406	426	8,883 33	0,000 0818	0,02 33	TTATAATTTCTCTT TTATTCT	JASPA R
RXRB	chr3:18033 2773-180333239	115	128	- 0,924 528	0,000 0821	0,07 29	TGCTTAAAAGGTC A	JASPA R
GFI1B	chr3:18033 2773-180333239	175	185	10,67 86	0,000 0844	0,07 35	CAACCTCAGAA	JASPA R
HLTF	chr3:18033 2773-180333239	357	366	9,093 02	0,000 0859	0,07 76	ACCCTTTTCC	JASPA R
ELK4	chr3:18033 2773-180333239	264	274	9,490 57	0,000 0862	0,07 62	GTATTTCCTGG	JASPA R
PITX3	chr3:18033 2773-180333239	226	234	10,81 48	0,000 0862	0,07 9	CTTAATCCT	JASPA R
MEIS1	chr3:18033 2773-180333239	53	59	10,45 45	0,000 0863	0,07 93	TTGACAG	JASPA R

SPIB	chr3:18033 2773- 180333239	349	355	11,41 86	0,000 0863	0,07 77	AGAGGAA	JASPA R
ELF4	chr3:18033 2773- 180333239	262	273	7,2	0,000 0926	0,08 29	GCCCAGGAAATA	JASPA R
EHF	chr3:18033 2773- 180333239	262	273	8,816 67	0,000 0945	0,08 44	GCCCAGGAAATA	JASPA R

Figure S1

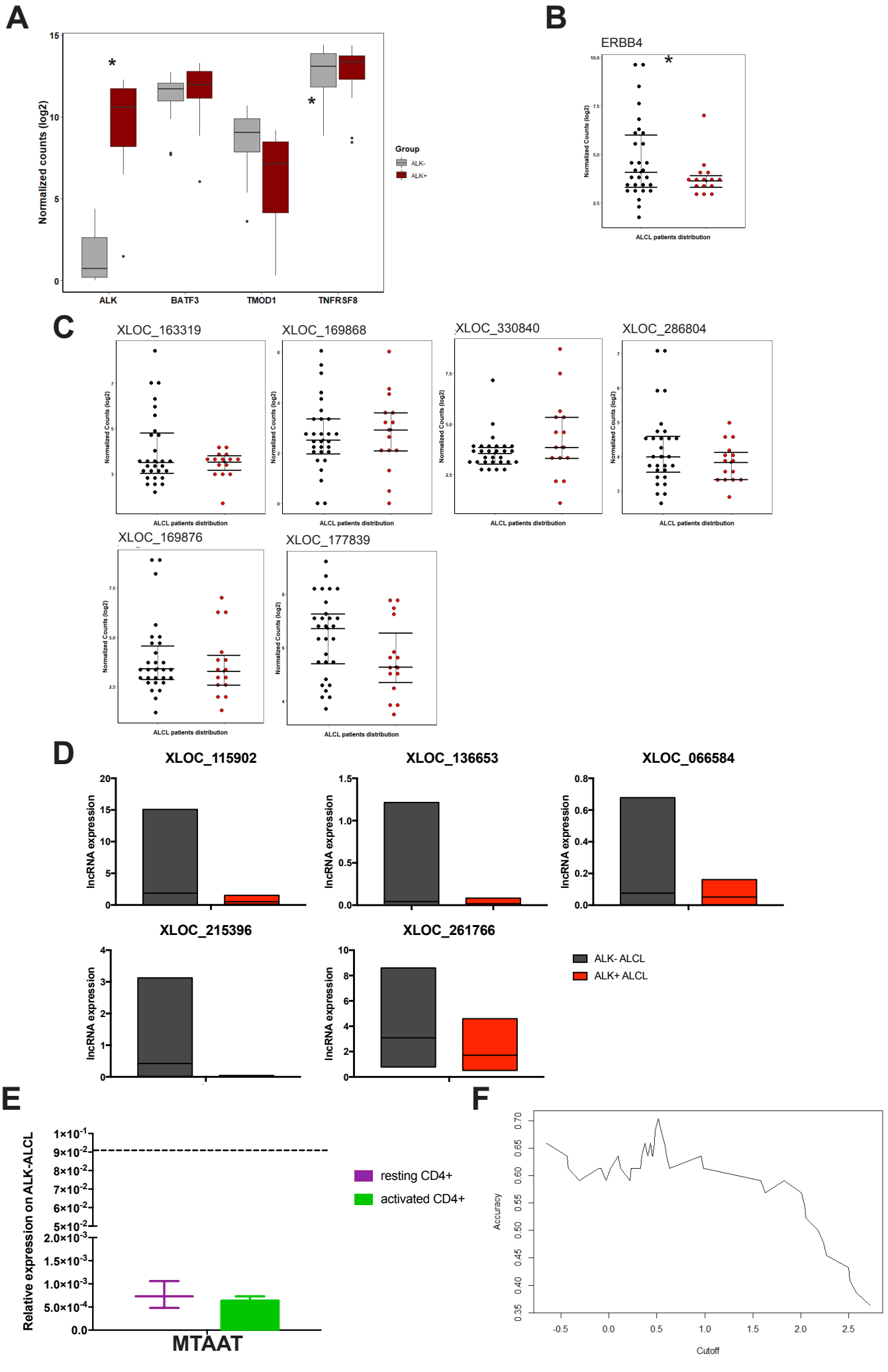
A
Normalized counts (log2)
Group
ALK-
ALK+
ALK
BATF3
TMOD1
TNFRSF8
B
ERBB4
Normalized Counts (log2)
ALCL patients distribution
C
XLOC_163319
XLOC_169868
XLOC_330840
XLOC_286804
XLOC_169876
XLOC_177839
D
XLOC_115902
XLOC_136653
XLOC_066584
XLOC_215396
XLOC_261766
lncRNA expression
ALK- ALCL
ALK+ ALCL
E
Relative expression on ALK-ALCL
resting CD4+
activated CD4+
MTAAT
F
Accuracy
Cutoff

Figure S2

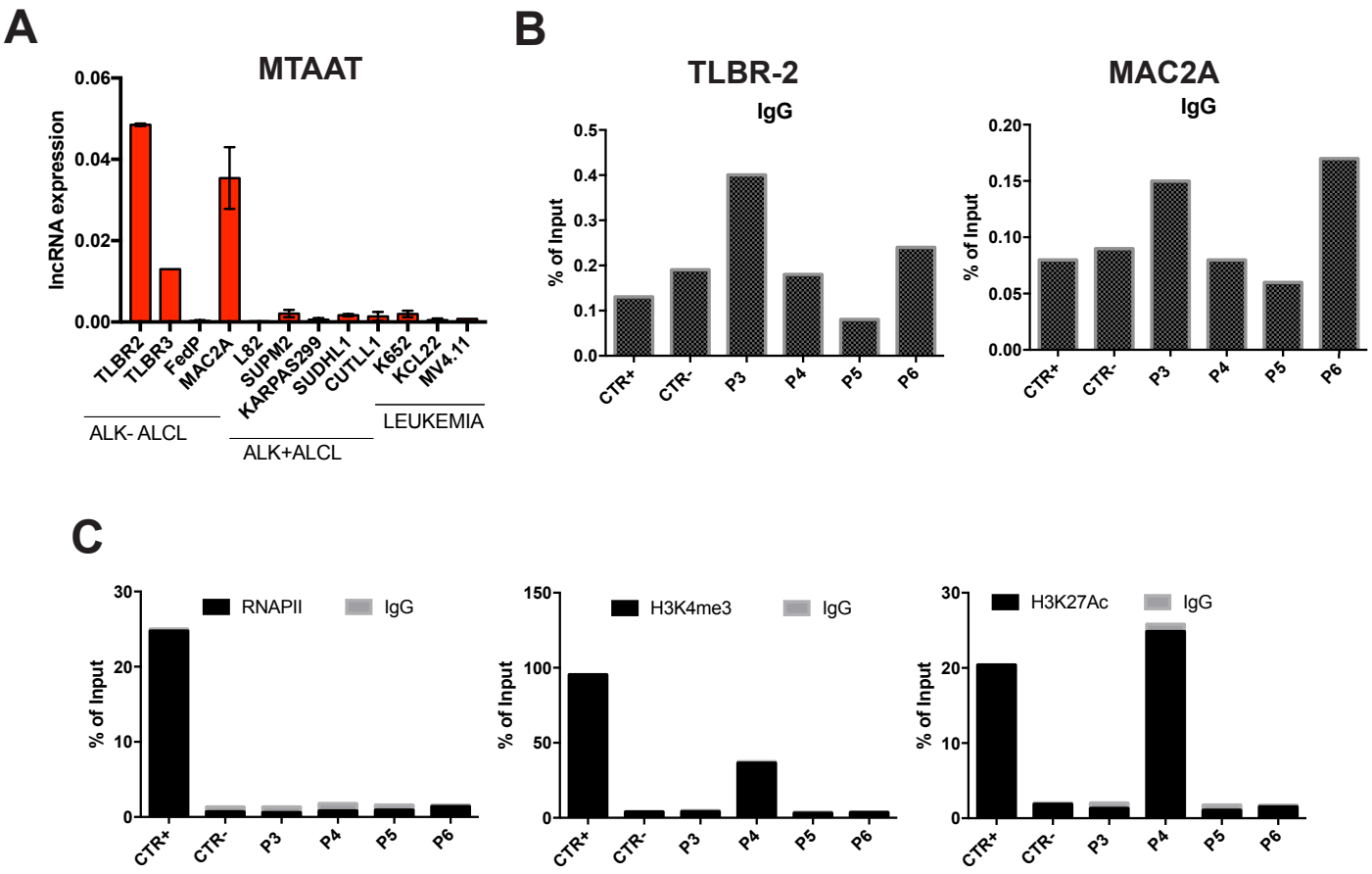
A
MTAAT
lncRNA expression
0.06
0.04
0.02
0.00
TLBR2
TLBR3
FedP
MAC2A
L82
SUPM2
KARPAS299
SUDHL1
CUTLL1
K652
KCL22
MV4.11
ALK- ALCL
ALK+ALCL
LEUKEMIA
B
TLBR-2
IgG
% of Input
0.5
0.4
0.3
0.2
0.1
0.0
CTR+
CTR-
P3
P4
P5
P6
MAC2A
IgG
% of Input
0.20
0.15
0.10
0.05
0.00
C
RNAPII
IgG
% of Input
30
20
10
0
H3K4me3
IgG
% of Input
150
100
50
0
H3K27Ac
IgG
% of Input
30
20
10
0

Figure S3

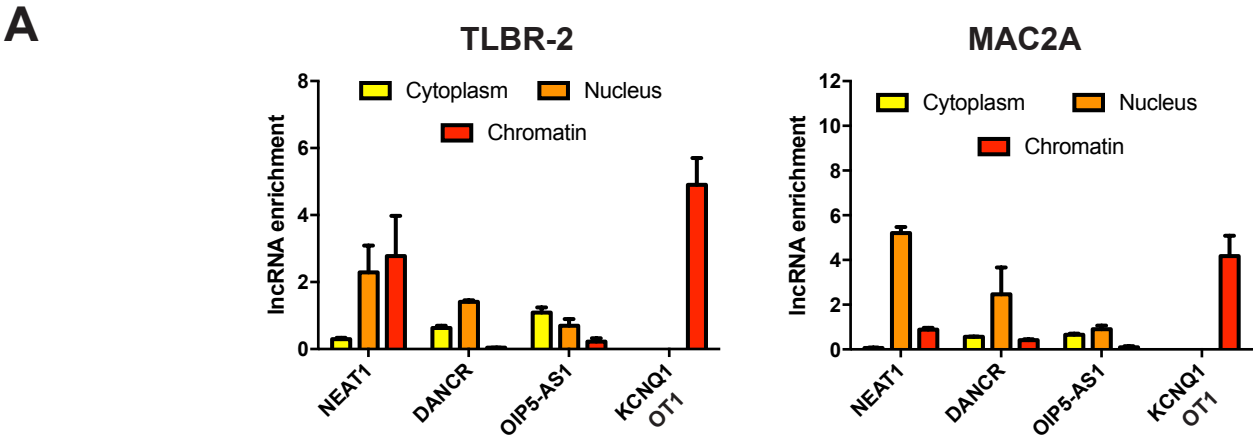
A
TLBR-2
MAC2A
Cytoplasm
Nucleus
Chromatin
lncRNA enrichment
NEAT1
DANCR
OIP5-AS1
KCNQ1 OT1

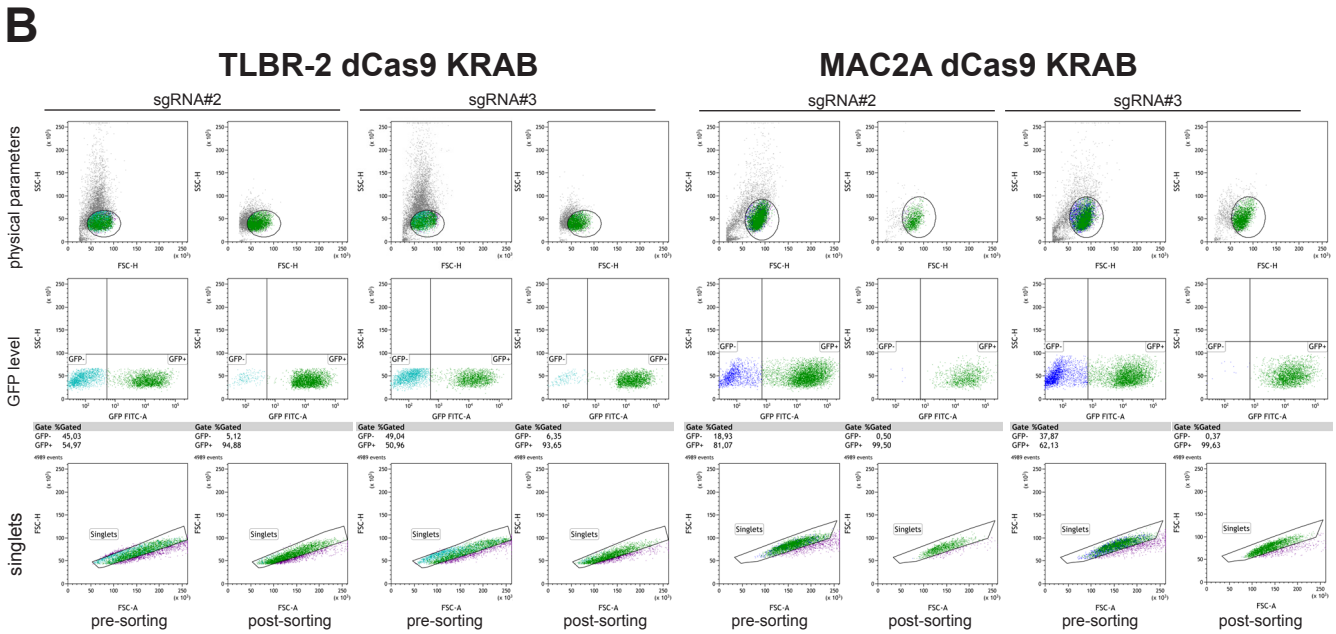
B
TLBR-2 dCas9 KRAB
MAC2A dCas9 KRAB
sgRNA#2
sgRNA#3
physical parameters
GFP level
singlets
pre-sorting
post-sorting

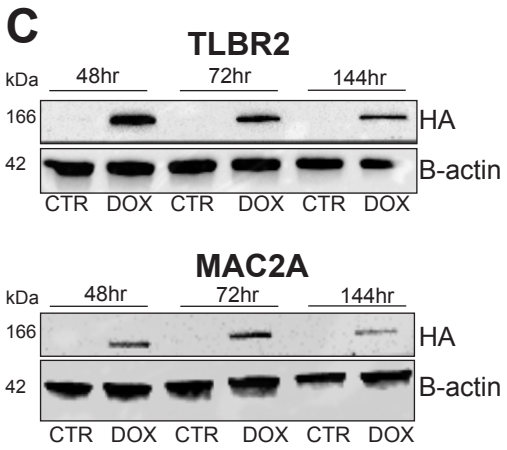
C
TLBR2
MAC2A
kDa
48hr
72hr
144hr
166
42
HA
B-actin
CTR
DOX

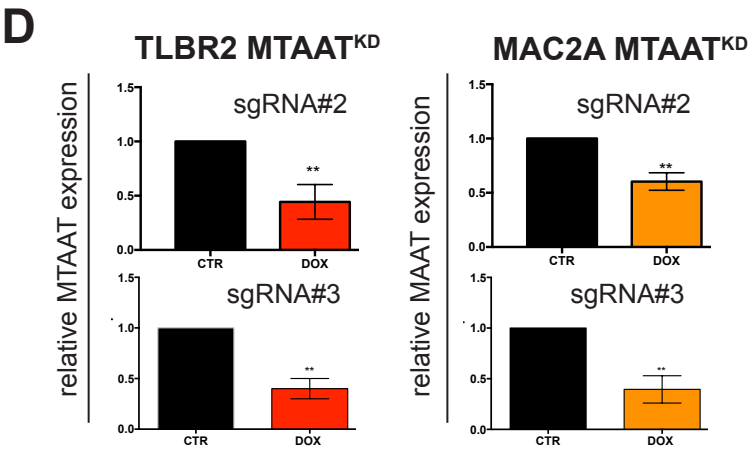
D
TLBR2 MTAAT^KD
MAC2A MTAAT^KD
relative MTAAT expression
relative MAAT expression
sgRNA#2
sgRNA#3
CTR
DOX

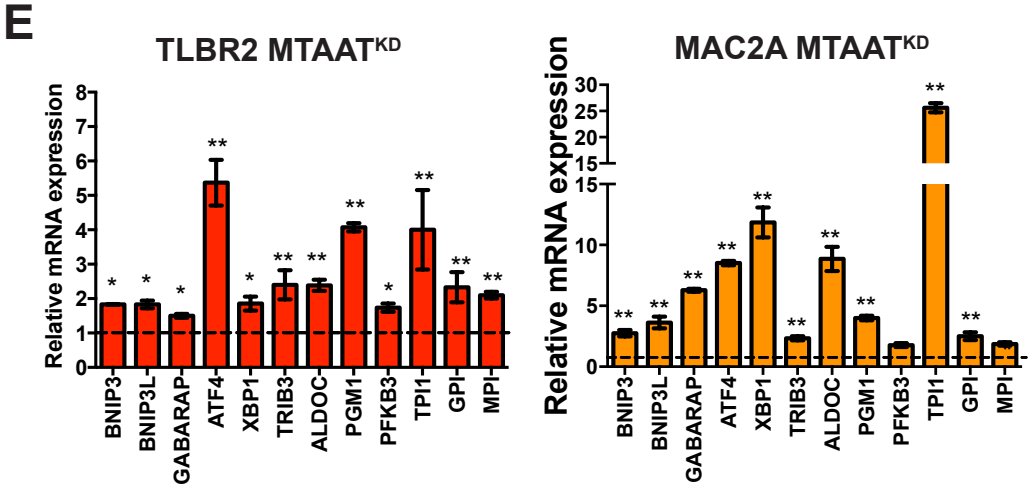
E
TLBR2 MTAAT^KD
MAC2A MTAAT^KD
Relative mRNA expression
BNIP3
BNIP3L
GABARAP
ATF4
XBP1
TRIB3
ALDOC
PGM1
PFKB3
TPI1
GPI
MPI

Figure S4

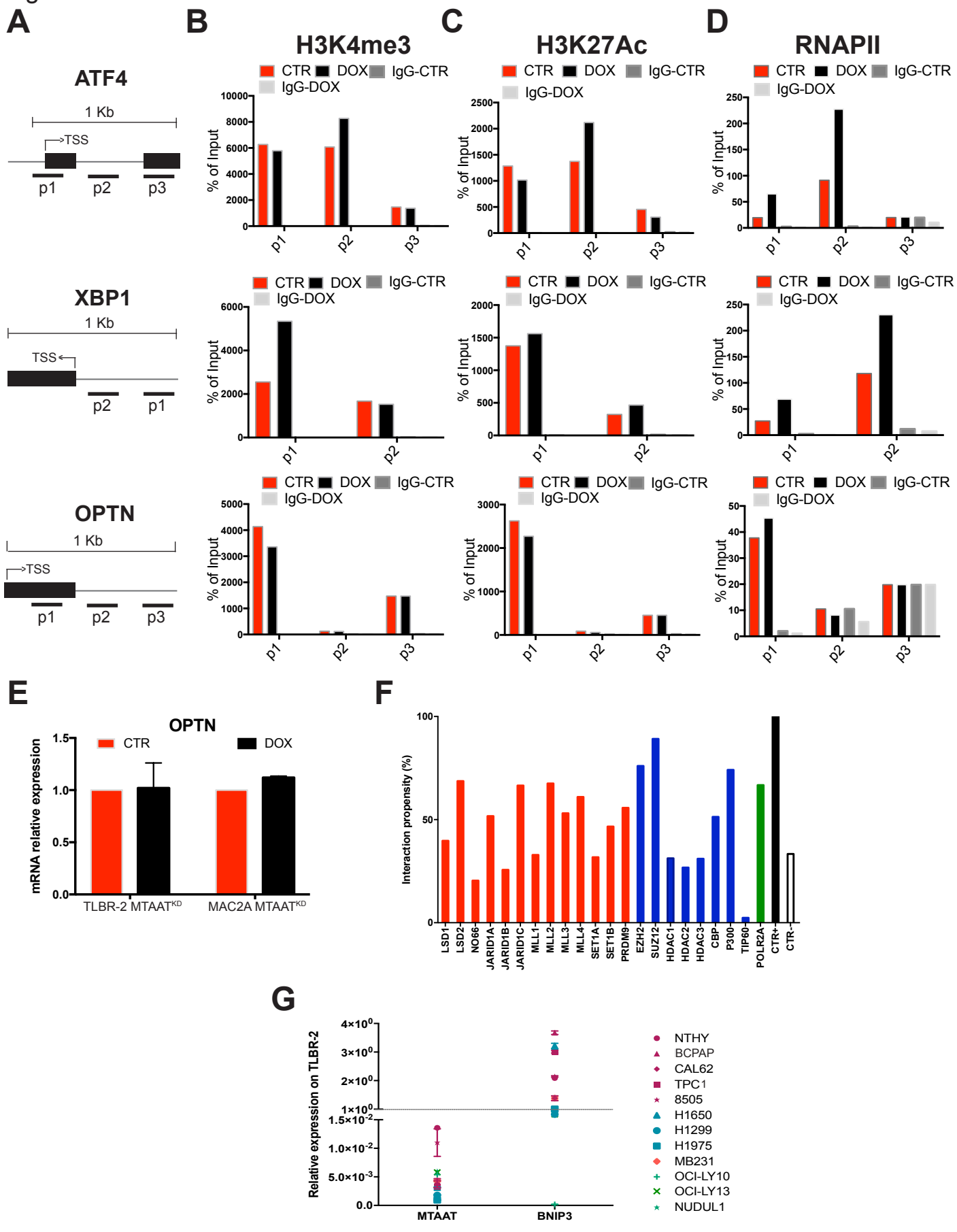
A
B
C
D
H3K4me3
H3K27Ac
RNAPII
ATF4
1 Kb
TSS
p1
p2
p3
XBP1
OPTN
CTR
DOX
IgG-CTR
IgG-DOX
% of Input
E
OPTN
mRNA relative expression
TLBR-2 MTAAT^KD
MAC2A MTAAT^KD
F
Interaction propensity (%)
LSD1
LSD2
NO66
JARID1A
JARID1B
JARID1C
MLL1
MLL2
MLL3
MLL4
SET1A
SET1B
PRDM9
EZH2
SUZ12
HDAC1
HDAC2
HDAC3
CBP
P300
TIP60
POLR2A
CTR+
CTR-
G
Relative expression on TLBR-2
MTAAT
BNIP3
NTHY
BCPAP
CAL62
TPC1
8505
H1650
H1299
H1975
MB231
OCI-LY10
OCI-LY13
NUDUL1

Figure S5

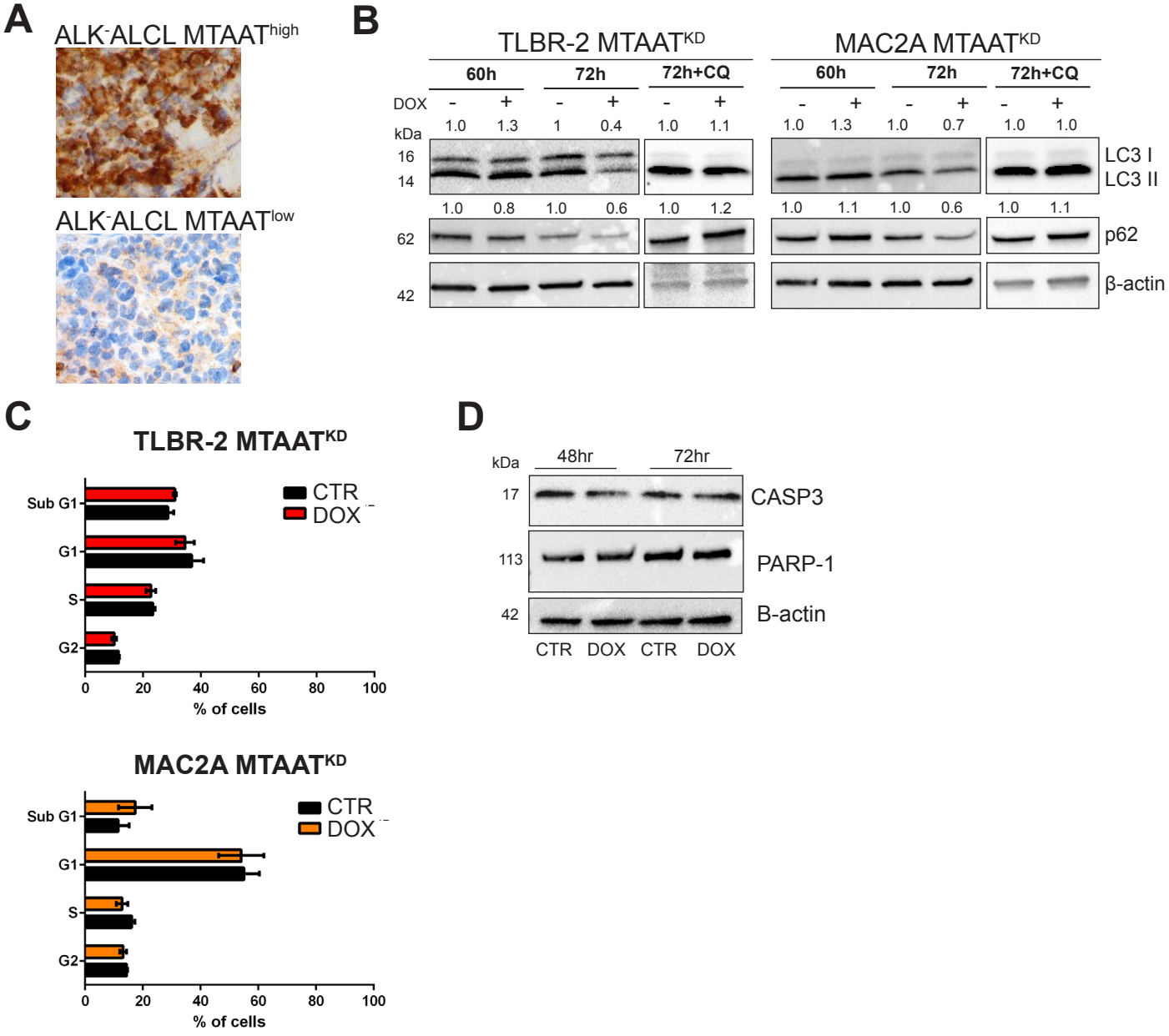
A
ALK-ALCL MTAAThigh
ALK-ALCL MTAATlow
B
TLBR-2 MTAATKD
MAC2A MTAATKD
60h
72h
72h+CQ
DOX
kDa
16
14
62
42
LC3 I
LC3 II
p62
β-actin
C
TLBR-2 MTAATKD
Sub G1
G1
S
G2
CTR
DOX
% of cells
MAC2A MTAATKD
D
48hr
72hr
17
113
CASP3
PARP-1
B-actin
CTR
DOX